iScience

CellPress
OPEN ACCESS

Article

Cholesterol-induced robust Ca oscillation in astrocytes required for survival and lipid droplet formation in high-cholesterol condition

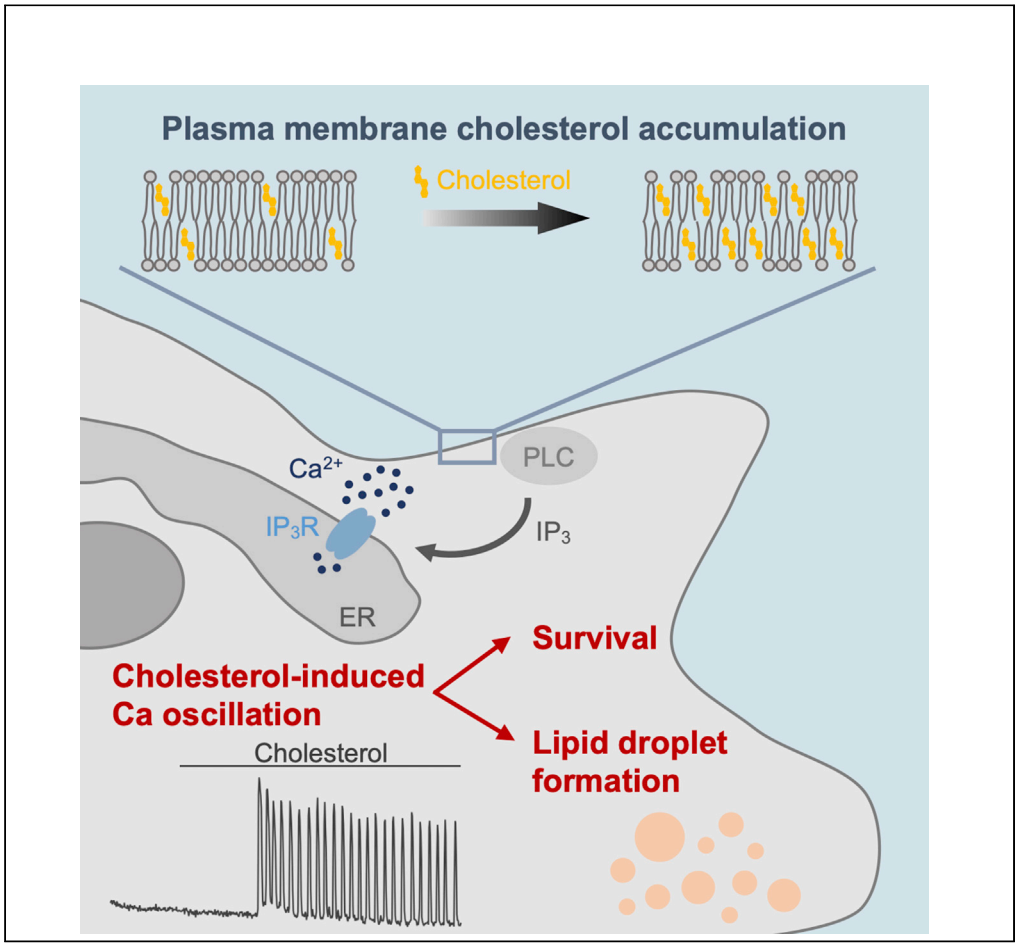

Chihiro Adachi,
Shio Otsuka,
Takafumi Inoue

inoue.t@waseda.jp

Highlights

Robust Ca oscillation by cholesterol in astrocytes but not in neurons and microglia

Cholesterol-induced Ca oscillation relates to membrane cholesterol accumulation

The Ca oscillation is driven via the PLC-IP_3 signaling pathway

Ca oscillation inhibition leads to astrocytic death and lipid droplet malformation

Adachi et al., iScience 25, 105138
October 21, 2022
https://doi.org/10.1016/j.isci.2022.105138

iScience

CellPress
OPEN ACCESS

Article

Cholesterol-induced robust Ca oscillation in astrocytes required for survival and lipid droplet formation in high-cholesterol condition

Chihiro Adachi,[1] Shio Otsuka,[1] and Takafumi Inoue[1,2,*]

SUMMARY

Cholesterol, one of the major cell membrane components, stabilizes membrane fluidity and regulates signal transduction. Beside its canonical roles, cholesterol has been reported to directly activate signaling pathways such as hedgehog (Hh). We recently found that astrocytes, one of the glial cells, respond to Hh pathway stimulation by Ca signaling. These notions led us to test if extracellularly applied cholesterol triggers Ca signaling in astrocytes. Here, we found that cholesterol application induces robust Ca oscillation only in astrocytes with different properties from the Hh-induced Ca response. The Ca oscillation has a long delay which corresponds to the onset of cholesterol accumulation in the plasma membrane. Blockade of the Ca oscillation resulted in enhancement of astrocytic cell death and disturbance of lipid droplet formation, implying a possibility that the cholesterol-induced Ca oscillation plays important roles in astrocytic survival and cholesterol handling under pathological conditions of cholesterol load such as demyelination.

INTRODUCTION

Cholesterol is a major constituent of the plasma membrane, where it forms lipid raft, cholesterol-rich domain. The concept of lipid raft has attracted attention owing to the accumulation of various receptors thereby serving as hot spots for signal transduction (Lingwood and Simons, 2010). Several G-protein coupled receptors (GPCRs) and tyrosine kinase receptor families possess cholesterol-binding domains termed cholesterol consensus motif (CCM) or cholesterol recognition amino acid consensus (CRAC) motifs, which are considered to stabilize the conformation toward active or inactive receptor states (Cannarozzo et al., 2021; Gimpl, 2016; Paila and Chattopadhyay, 2010). On the other hand, direct activation of signaling pathways by cholesterol binding to effectors has been reported for some GPCRs. Smoothened, a receptor residing in the hedgehog (Hh) signaling pathway, has two cholesterol binding sites, and in addition to the authentic modulation of the receptor function, cholesterol directly activates smoothened and the downstream transcription factor Gli (Deshpande et al., 2019; Huang et al., 2016a; Luchetti et al., 2016).

Hh is a well-known morphogen in organogenesis and neurogenesis during development. In addition to the canonical Hh signaling pathway that activates Gli, non-canonical pathways not linked to Gli have been proposed: namely Type I non-canonical Hh signaling that originates from Patched1, a Hh receptor, but is unrelated to Gli activation through smoothened activation and Type II non-canonical Hh signaling that activates trimeric Gi proteins through smoothened activation (Adachi et al., 2019; Brennan et al., 2012; Jenkins, 2009). We recently identified another non-canonical Hh pathway where Sonic hedgehog, a Hh ligand, and smoothened agonist (SAG) evoke calcium (Ca) response in astrocytes (Adachi et al., 2019), in which smoothened activation, inositol trisphosphate (IP_3) production and intracellular Ca release were required. In the course of investigation of this phenomenon, we found that extracellularly applied cholesterol evoked Ca oscillation in astrocytes through the phospholipase C (PLC) and IP_3 receptor pathway with different characteristics from the Hh-induced Ca response. Histochemical characterization revealed that neurons and microglia did not respond to applied cholesterol by Ca response. The uprise timing of cholesterol accumulation in the plasma membrane was close to the Ca response lag. Blockade of the cholesterol-induced Ca oscillation resulted in decrease in lipid droplet formation and increased cell death of astrocytes. These results suggest that cholesterol may serve as a signal transducer which directly activates an

[1]Department of Life Science and Medical Bioscience, School of Advanced Science and Engineering, Waseda University, Tokyo 162-8480, Japan

[2]Lead contact

*Correspondence: inoue.t@waseda.jp

https://doi.org/10.1016/j.isci.2022.105138

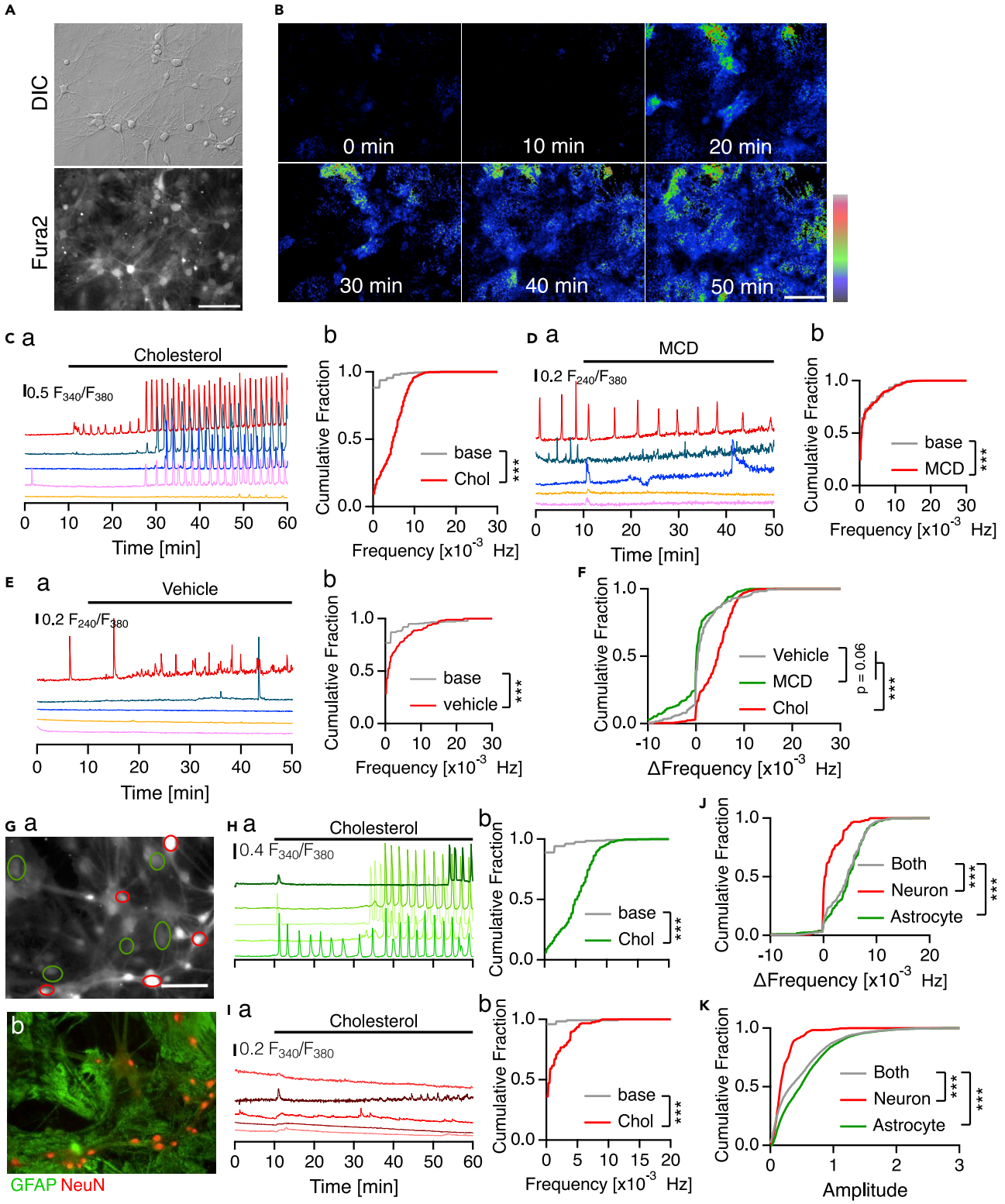

Figure 1. Ca oscillation evoked by extracellularly applied cholesterol in astrocytes in mouse hippocampal primary culture

(A) Mouse hippocampal primary culture. Top, a differential interference contrast image; bottom, fluorescence image with Fura-2. Scale bar, 100 μm.

(B) F_{340}/F_{380} ratio images of the same field of view in A along time. Scale bar, 100 μm.

Figure 1. *Continued*

(C–E) Typical time-course traces of Fura-2 F_{340}/F_{380} ratio values (a) from cells incubated in 250 μM cholesterol (C), in 2.5 mM MCD only (D), and in vehicle (E), and cumulative fraction of Ca oscillation frequency (b). ***p<0.001, Mann-Whitney U test.

(F) Cumulative fraction of ΔFrequency calculated from vehicle [number of cell(number of culture); 174(3)], MCD [412(5)] and cholesterol treated groups [498(6)]. ***p<0.001, Kruskal-Wallis test and post hoc Bonferroni corrected Mann-Whitney U test.

(G) Mouse primary hippocampal culture stained with Fura-2 (a) and stained with anti-NeuN (red) and anti-GFAP (green) antibodies post hoc (b), showing the same field of view. Red and green ROIs in (a) represent NeuN-positive (neuron) and GFAP-positive (astrocyte) cells, respectively. Scale bar, 100 μm.

(H and I) Ca imaging traces (a) and cumulative fraction of Ca oscillation frequency during the periods before (baseline) and after (Chol) cholesterol application (b) in astrocytes (H) and neurons (I). The time course traces of Ca changes are overlaid with arbitrary vertical shifts. ***p<0.001, Mann-Whitney U test.

(J and K) Cumulative fractions of ΔFrequency (J) and amplitude of Ca transients (K) from all cell types (Both), neurons (n = 119 cells), and astrocytes (n = 379 cells). ***p<0.001, Kruskal-Wallis test and post hoc Bonferroni corrected Mann-Whitney U test.

See also Figures S1 and S2 and Video S1.

unknown signaling pathway that induces Ca oscillation in astrocytes. And the Ca signaling may protect astrocytes from cell death under high cholesterol conditions, such as demyelinating diseases.

RESULTS

Cholesterol/MCD complex induces Ca oscillation only in astrocytes in primary hippocampal culture

To test effects of extracellular cholesterol load to cells in the brain, we applied cholesterol extracellularly to hippocampal primary culture cells and responses were monitored by Ca imaging (Figure 1A). Because cholesterol is insoluble in water, it was conjugated with methyl-β-cyclodextrin (MCD). MCD binds with cholesterol and acts as a water-soluble cholesterol donor (Zidovetzki and Levitan, 2007). After a 10 min baseline period, cells were exposed to a cholesterol/MCD solution (250 μM cholesterol and 2.5 mM MCD, 1:10 molar ratio), and most of the cells exhibited strong Ca oscillation 10–20 min after the exposure (Figures 1B and 1C, Video S1). During the 50-min period following the exposure, more than 90% of the cells manifested Ca transients (Figure 1Cb). MCD alone did not evoke such Ca oscillation; only spontaneous Ca transients were observed in some cells, which were also observed before the MCD application and in vehicle-treated control cells (Figures 1D and 1E). Ca response was evaluated by the frequency of Ca transients. Ca event frequency was compared among treatments after subtracting Ca event frequency during the baseline period from that after drug application in each cell (ΔFrequency; Adachi et al., 2019). Control vehicle-treated cells and MCD-treated cells showed similar ΔFrequency distributions, while cholesterol-treated cells showed an apparent increase in ΔFrequency (right shift in the cumulative curve, Figure 1F), indicating that extracellular cholesterol application induces robust Ca oscillation in hippocampal cells.

Because the primary culture contained neurons and glial cells, we examined the relationship between the cholesterol-induced Ca oscillations and neuronal excitability. Under 1 μM tetrodotoxin (TTX), a Na channel blocker, cholesterol induced Ca oscillation with even higher frequencies and smaller amplitudes than those without TTX (Figure S1), suggesting that neuronal excitability has some influence on the cholesterol-induced Ca oscillation. Next, we performed Ca imaging combined with post hoc immunohistochemistry to identify the responsible cell types. All the cells were stained either by anti-NeuN or by anti-glial fibrillary acidic protein (GFAP) antibodies (Figure 1G), in agreement with our previous study that the cell population of our hippocampal primary culture preparation is composed mostly of neurons and astrocytes, and that other cell types, such as oligodendrocytes and microglia, are ignorable (Adachi et al., 2019). GFAP-positive cells, namely astrocytes, exhibited cholesterol-induced Ca oscillation (Figure 1H), whereas NeuN-positive cells, neurons, responded to cholesterol with occasional small Ca transients (Figure 1I). The brown trace in Figure 1Ia shows a periodic signal fluctuation of low amplitude, which we consider to be a crosstalk of the strong fluorescence changes emitted from the overlapping astrocyte because the events in the neuron and the astrocyte are synchronized. The distribution patterns of ΔFrequency and Ca event amplitude of astrocytes both overlapped well with those of all cell populations, whereas those of neurons completely differed (Figures 1J and 1K). This apparent difference in Ca response between astrocytes and neurons promoted us to ask how general is this cholesterol-induced Ca response among cell types. We tested popular cell lines, C6, COS-7, HEK293T, HeLa, and NIH3T3, and none showed any Ca response to bath applied cholesterol (Figure S2). It was unexpected that the C6 cell line did not respond to cholesterol, because it is derived from rat glioma and shares many features with primary cultured astrocytes (Galland et al., 2019). These results suggest that the cholesterol-induced Ca oscillation is not a general response but rather limited in astrocytes and a small number of cell types, if any.

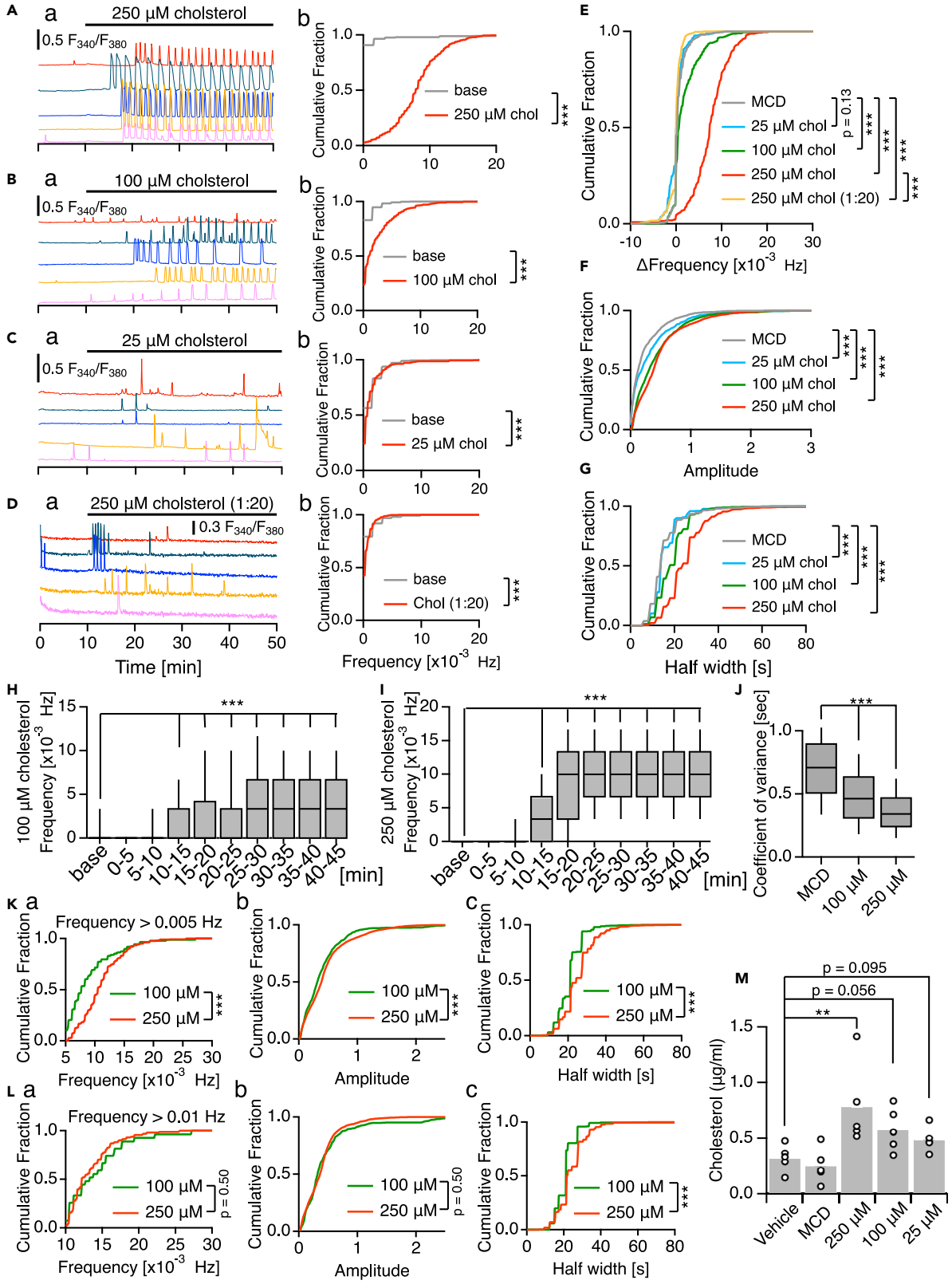
A
a
250 µM cholsterol
0.5 F340/F380
b
Cumulative Fraction
base
250 µM chol
***
B
a
100 µM cholsterol
0.5 F340/F380
b
base
100 µM chol
***
C
a
25 µM cholsterol
0.5 F340/F380
b
base
25 µM chol
***
D
a
250 µM cholsterol (1:20)
0.3 F340/F380
Time [min]
b
base
Chol (1:20)
***
Frequency [x10-3 Hz]
E
MCD
25 µM chol
100 µM chol
250 µM chol
250 µM chol (1:20)
p = 0.13
***
ΔFrequency [x10-3 Hz]
F
MCD
25 µM chol
100 µM chol
250 µM chol
Amplitude
G
MCD
25 µM chol
100 µM chol
250 µM chol
Half width [s]
H
100 µM cholesterol Frequency [x10-3 Hz]
***
base
0-5
5-10
10-15
15-20
20-25
25-30
30-35
35-40
40-45
[min]
I
250 µM cholesterol Frequency [x10-3 Hz]
***
[min]
J
Coefficient of variance [sec]
***
MCD
100 µM
250 µM
K
a
Frequency > 0.005 Hz
100 µM
250 µM
***
Frequency [x10-3 Hz]
b
Amplitude
c
Half width [s]
L
a
Frequency > 0.01 Hz
p = 0.50
b
c
M
p = 0.095
p = 0.056
**
Cholesterol (µg/ml)
Vehicle
MCD
250 µM
100 µM
25 µM

Figure 2. Varying Ca response with cholesterol concentrations in hippocampal astrocyte culture

(A–D) Ca imaging traces (a) stimulated with 250 (A), 100 (B) and 25 (C) μM cholesterol (1:10 cholesterol/MCD molar ratio) and 250 μM cholesterol (1:20 cholesterol/MCD, D), and distribution of Ca event frequency (b). ***p<0.001, Mann-Whitney U test.

(E–G) ΔFrequency (E), amplitude (F) and half-width (G) of Ca events. Number of cells(number of cultures): MCD, 469(5); 25 μM cholesterol, 369(5); 100 μM cholesterol, 517(6); 250 μM cholesterol, 350(5); 100 μM cholesterol (plateau phase), 277(6); 250 μM cholesterol (plateau phase), 319(5). ***p<0.001, Kruskal-Wallis test and post hoc Bonferroni corrected Mann-Whitney U test.

(H and I) Transition of the Ca event frequency with 100 (H) and 250 (I) μM cholesterol. ***p<0.001, Kruskal-Wallis test and post hoc Bonferroni corrected Mann-Whitney U test.

(J) Coefficient of variance of Ca event intervals during plateau phases (15–45 min, 25–45 min, and all periods for 250 and 100 μM cholesterol and sole MCD, respectively). ***p<0.001, Kruskal-Wallis test and post hoc Bonferroni corrected Mann-Whitney U test.

(K and L) Frequency (a), amplitude (b), and half-width (c) of Ca events in astrocytes incubated with 100 and 250 μM cholesterol during the plateau period in cells with high-frequency Ca oscillation (>0.005 Hz, n = 73 and 275 cells for 100 and 250 μM cholesterol, respectively, in K; > 0.01 Hz, n = 15 and 92 cells for 100 and 250 μM cholesterol, respectively, in L). ***p<0.001, Mann-Whitney U test.

(M) Quantification of total free cholesterol, n = 5. **p<0.01, Mann-Whitney U test.

See also Figures S3–S5.

Features of cholesterol-induced Ca oscillation in astrocytes

Because astrocytes turned out to be the player of the cholesterol-induced Ca oscillation, we hereafter used primary astrocyte-rich glial cultures to characterize the phenomenon. Ca oscillation was induced in almost all cells in hippocampal glial culture with 250 μM cholesterol (Figure 2A), similarly to the primary neuron-astrocyte mixed culture (Figure 1). With 100 μM cholesterol, more than 60% of the cells showed Ca oscillation (Figure 2B), and no Ca oscillatory response was observed with 25 μM cholesterol (Figure 2C) and with 2.5 mM MCD without cholesterol (not shown). Cholesterol (250 μM) of cholesterol/MCD complex at 1:20 ratio, the ratio at which MCD is known to become saturated with cholesterol, did not induce strong Ca oscillation in astrocytes (Figure 2D) as seen with 1:10 cholesterol/MCD complex (Figure 2A). ΔFrequency of Ca oscillation showed marked and moderate increases in the 250 and 100 μM cholesterol treated cells, respectively, compared to those of the 25 μM cholesterol, the sole MCD application and the 250 μM 1:20 cholesterol treatment (Figure 2E). The amplitude and half-width of Ca transients in 250 μM cholesterol were the largest, followed by 100 and 25 μM cholesterol, and MCD alone (Figures 2F and 2G). The Ca response had a 5–10 min lag to cholesterol application and reached a plateau frequency level within 15 and 25 min with 250 and 100 μM cholesterol, respectively (Figures 2H and 2I). During the plateau phases, the coefficient of variance of the Ca transient intervals was smaller in astrocytes treated with 100 and 250 μM cholesterol than that in MCD-treated control cells during a corresponding time range (Figure 2J), indicating that the interval of cholesterol-induced Ca oscillation was more regular under cholesterol. When cells with Ca oscillation frequencies greater than 0.005 Hz during these periods were selected, the distribution pattern of Ca event frequency of the 100 and 250 μM cholesterol groups became closer (Figure 2Ka), and mostly overlapped when the threshold was raised to 0.01 Hz (Figure 2La). The distribution of Ca event amplitudes of the 100 and 250 μM cholesterol groups overlapped with either frequency threshold (Figures 2Kb and 2Lb). Half-width of Ca transients was slightly longer in the 250 μM cholesterol group than in the 100 μM group (Figures 2Kc and 2Lc). These results suggest that the frequency of cholesterol-induced Ca oscillation has an upper limit, which was reached in most cells in 250 μM cholesterol, and in fewer cells in 100 μM cholesterol with longer delay than in 250 μM. In accordance with these results, free cholesterol quantity in cultured astrocytes was raised by 2- to 3-fold after 30 min incubation with 250 μM cholesterol compared with the vehicle control (Figure 2M). These properties of cholesterol-induced Ca oscillation seemed to be limited to hippocampal astrocytes: whereas primary astrocytes prepared from cortex and spinal cord, in which astrocytes predominated (Figure S3), also displayed cholesterol-induced Ca oscillation, the frequency and responding cell population were much smaller than those of hippocampal astrocytes (Figure S4). Post hoc immunostaining revealed that the Ca responses observed in the spinal cord culture was most represented by astrocytes, and the contribution of microglia, Iba1-positive cells, to the cholesterol-induced Ca oscillation was very small (Figures S4E–S4I). These results suggest that cholesterol-induced Ca oscillation may occur in astrocytes with different properties depending on the brain area. Hereafter, we used hippocampal astrocytes and 250 μM cholesterol, which showed stable Ca oscillations.

Differences between Hh- and cholesterol-induced Ca responses

We compared the cholesterol-induced Ca oscillation to the SAG-induced Ca response that we reported previously (Adachi et al., 2019). The Ca imaging data obtained from mouse hippocampal astrocyte culture in the previous study were reanalyzed with the same parameters used for the cholesterol-induced Ca

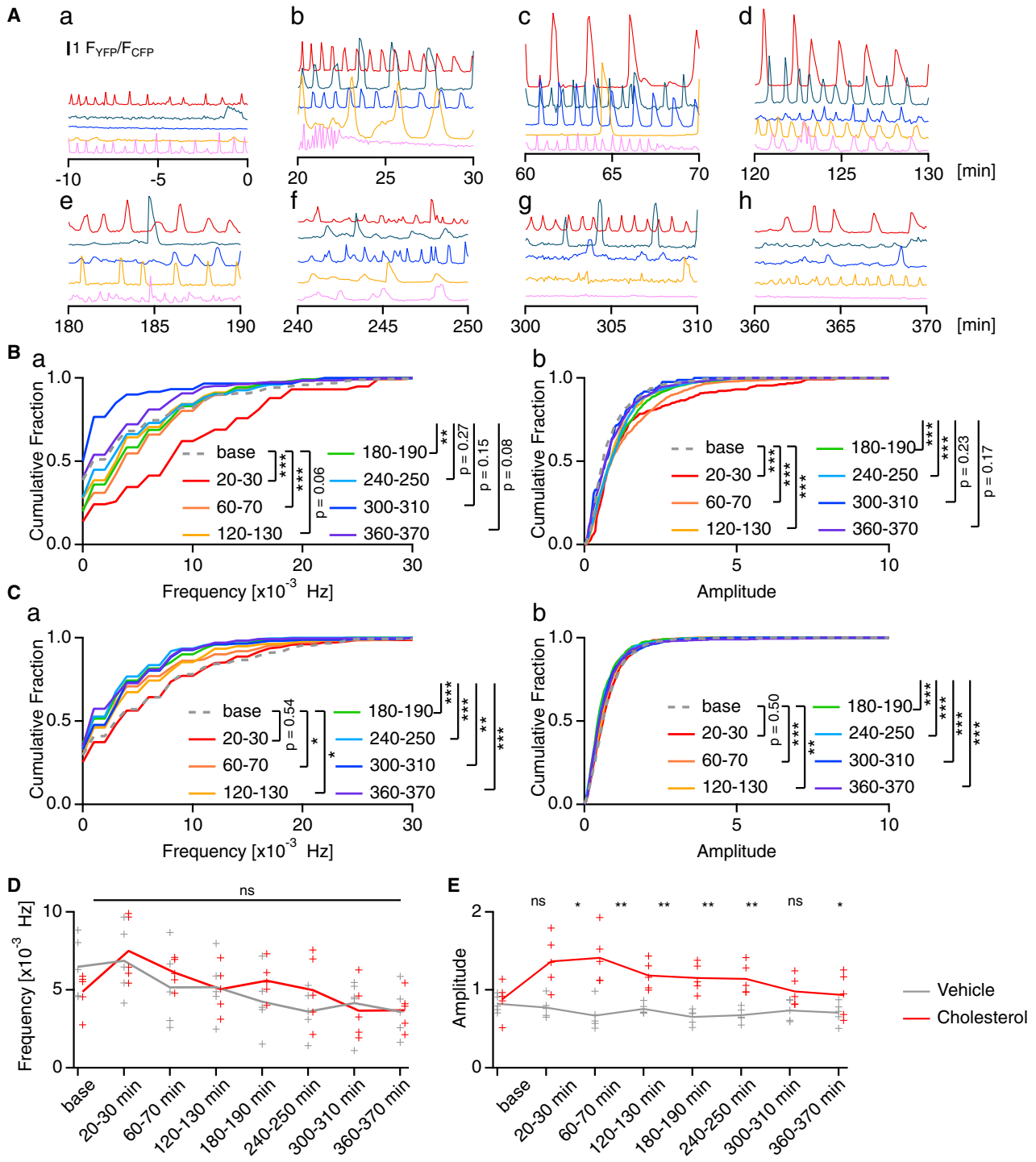

Figure 3. Ca oscillation lasts at least 4 h in the presence of cholesterol

(A) Ca imaging traces from Cameleon(YC3.60)-expressing astrocytes. Ca imaging was performed for 10 min before (baseline, a) and 20 min after cholesterol application (b). Thereafter, 10 min Ca imaging was done every 1 h (c–h) from different field of views each time.

(B and C) Cumulative fractions of frequency (a) and amplitude (b) of Ca events with 250 μM cholesterol (B) and vehicle (C). *p<0.05, **p<0.01, ***p<0.001, Mann-Whitney U test.

(D and E) Time course of frequency (D) and amplitude (E) of Ca events with cholesterol (red) and vehicle (gray). '+' represents the average of cells in each culture batch, and lines show average of 5 batches. *p<0.05, **p<0.01, two-way repeated measures ANOVA and post hoc Steel-Dwass tests. Number of cells(number of cultures): cholesterol (base), 292(5); cholesterol (20–30 min), 295(5); cholesterol (60–70 min), 309(5); cholesterol (120–130 min), 309(5);

Figure 3. *Continued*
cholesterol (180–190 min), 353(5); cholesterol (240–250 min), 296(5); cholesterol (300–310 min), 285(5); cholesterol (360–370 min), 269(5); vehicle (base), 324(5); vehicle (20–30 min), 284(5); vehicle (60–70 min), 261(5); vehicle (120–130 min), 273(5); vehicle (180–190 min), 272(5); vehicle (240–250 min), 262(5); vehicle (300–310 min), 258(5); vehicle (360–370 min), 235(5).

oscillation in this study. The oscillation frequency in the cholesterol-induced Ca oscillation was much higher than that in the SAG-induced one with slightly larger amplitude (Figure S5A). The SAG-induced Ca response was completely blocked by a connexin gap junction and hemichannel inhibitor, carbenoxolone (CBX), indicating that it relies on the gap junction and/or hemi-channel activity (Adachi et al., 2019), whereas CBX only partially blocked the cholesterol-induced Ca oscillation (Figure S5B). These differences suggest that the features and underlying mechanisms of the cholesterol-induced Ca oscillation do not coincide with those of the SAG-induced Ca response, yet some are shared.

Long lasting cholesterol-induced Ca oscillation

Because the Ca oscillation under extracellular cholesterol appeared constant and did not decay for at least 30 min (Figure 2Aa), we examined the duration the Ca oscillation holds in the presence of cholesterol. For long-term Ca imaging, a protein-based Ca indicator, YC3.60, was expressed in astrocytes instead of loading Fura2, and culture medium containing 25 mM HEPES (pH 7.40) was used instead of HEPES-buffered saline (HBS). During the baseline period before cholesterol application, much more spontaneous Ca transients were observed than with HBS, presumably because of the presence of serum in the medium (Figure 3Aa). In this active spontaneous Ca activity background, cholesterol (250 μM) induced Ca oscillation of larger amplitudes than the baseline Ca transients with approximately 15 min lags, which lasted for the recording period up to 6 h (Figures 3AB–3H). Both the frequency and amplitude of Ca oscillation were highest around 20–30 min after cholesterol application and gradually decreased (Figures 3B, 3D, and 3E). Because long exposure of astrocytes to MCD without cholesterol, which was used as a control in previous experiments, reduced the viability of cells, vehicle (water) was used as a control. The time course of frequency decay was similar between the cell groups with or without cholesterol, except for the initial increase in the cholesterol-stimulated group. The increase in amplitude by cholesterol lasted for at least 4 h, whereas the Ca transient amplitude was constant in the control group (Figures 3B, 3C and 3E), thus we conclude that the cholesterol-induced Ca oscillation lasts for at least 4 h in the presence of cholesterol.

Washout of extracellular cholesterol enhances Ca oscillation

We found that washout of extracellularly applied cholesterol activates Ca responses in astrocytes. After a 10-min baseline in HBS, cholesterol was added to the bath, then, after 30 min incubation, it was washed out by superfusing HBS. This washout induced immediate enhancement rather than cessation of Ca oscillation evoked by the cholesterol (Figure 4A). The frequency of Ca events peaked during 0–30 min after washing and decreased gradually (Figure 4C). MCD without cholesterol conjugation did not show such Ca frequency increase after washout (Figures 4B and 4D).

Cholesterol accumulation in the plasma membrane may drive Ca oscillation

The observation that the Ca oscillation did not cease by washout of extracellular cholesterol hinted that the oscillation is driven not by direct action of extracellular cholesterol molecules to the cell surface but by cholesterol molecules newly embedded in the plasma membrane. Cholesterol level in the plasma membrane was examined using the filipin dye, which stains cholesterol mainly in the plasma membrane (Norman et al., 1972). Filipin signal gradually increased 10 min after cholesterol application, while it stayed at a lower level in vehicle-, MCD-, and 1:20 cholesterol/MCD-treated astrocytes (Figures 5A and 5B). The similarity of the timing that this filipin signal uprises and the 10-min lag of the cholesterol-induced Ca oscillation (Figure 2A) implies that the Ca oscillation may be ignited by cholesterol accumulated in the plasma membrane. Cholesterol content in the plasma membrane was kept high with 1:10 cholesterol after 24 h incubation (Figure 5B). When extracellular cholesterol was washed after 30 min incubation, the accumulated membrane cholesterol gradually decreased during the first 6 h and returned to the original level 24 h after the wash (Figure 5C).

Cholesterol-induced Ca oscillation requires the PLC-IP_3 pathway

To investigate the molecular mechanisms underlying the cholesterol-induced Ca oscillations in astrocytes, pharmacological experiments were performed. Astrocytes are well known for Ca responses by various

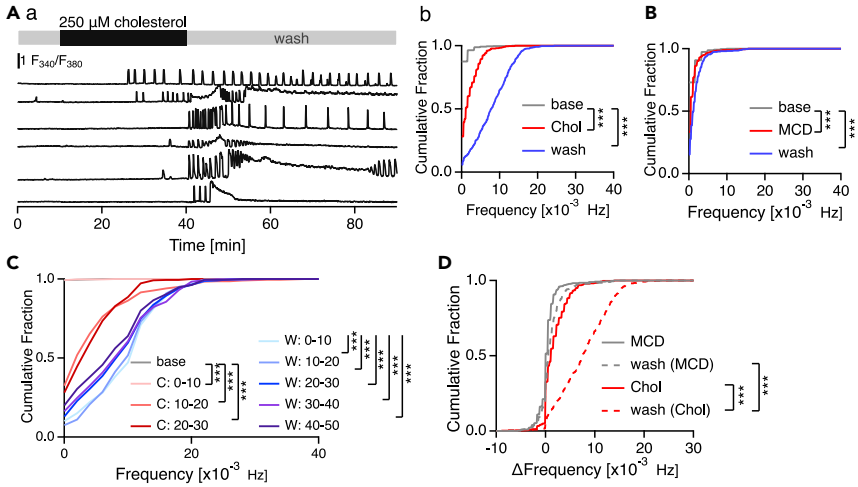

Figure 4. Cholesterol washout enhances cholesterol-induced Ca oscillation

(A) After 30 min incubation in cholesterol, extracellular cholesterol was removed by wash. Typical Ca time course traces (a) and cumulative frequency of Ca oscillation taken before (before), during (Chol) and after cholesterol incubation (wash) (b) are indicated. ***p<0.001, Mann-Whitney U test.

(B) Cumulative frequency of Ca events in control experiments where MCD without cholesterol conjugation was applied. ***p<0.001, Mann-Whitney U test.

(C) Cumulative fraction of Ca event frequency in cholesterol-treated cells calculated for 10 min time windows [baseline period (base), cholesterol incubation (C) and after wash (W)]. ***p<0.001, Mann-Whitney U test.

(D) Cumulative fraction of ΔFrequency before and after wash of cholesterol (Chol) and MCD alone (MCD). ***p<0.001, Kruskal-Wallis test and post hoc Bonferroni corrected Mann-Whitney U test. Number of cells(number of cultures): cholesterol, 394(5); MCD, 388(5).

stimuli, where Ca is mobilized from the extracellular space and from intracellular Ca stores. In the latter, sarco/ER Ca^{2+}-ATPase (SERCA) pumps Ca^{2+} into ER and IP_3 receptor and ryanodine receptor release the stored Ca^{2+} into cytosol. When astrocytes were preincubated with 2-aminoethoxydiphenyldorane (2-APB, 50 μM), an IP_3 receptor inhibitor, the cholesterol-induced Ca oscillation was completely blocked (Figure 6A). Thapsigargin (Tg, 100 nM), a SERCA inhibitor, also inhibited Ca oscillation (Figure 6B). These results indicate that intracellular Ca release from ER through IP_3 receptor is the key Ca source for the cholesterol-induced Ca oscillation. When astrocytes were preincubated with U-73122 (10 μM), an inhibitor of phospholipase C (PLC), which produces IP_3, U-73122 itself evoked temporal Ca transients for several minutes, and following cholesterol application did not evoke Ca oscillation (Figure 6C). U-73343, an inactive analog of U-73122 did not inhibit the cholesterol-induced Ca oscillation (10 μM, Figures 6Cb and 6Cc). Without extracellular Ca, where 1 mM EGTA was added to Ca-free HBS, astrocytes showed cholesterol-induced Ca oscillation with prolonged intervals and smaller amplitudes compared to Ca oscillations evoked in Ca-containing HBS, but still with larger ΔFrequency than the MCD-applied control group in Ca-free medium (Figure 6D). These results indicate that the PLC-IP_3 receptor pathway is the main source of Ca in the cholesterol-induced Ca oscillation.

Cholesterol increases Ca event frequency in astrocytes in acute hippocampal slice

Cultured astrocytes have different morphologies and features, including gene expression patterns, from those in the brain (Lange et al., 2012; Zhang and Barres, 2010). We asked if extracellularly applied cholesterol induces Ca responses in astrocytes in acute brain slice preparation, where the properties of astrocytes are closer to those in the brain. After 1–2 h incubation in 250 μM cholesterol, Ca imaging was conducted in dentate gyrus in hippocampal slices prepared from *Mlc1*-tTA:tetO-YC-Nano50 double transgenic (Mlc1-YC-Nano50) mice, in which a protein-based Ca indicator, YC-Nano50, is expressed under an astrocyte-specific *Mlc1*-tTA expression system (Figure 7Aa; Kanemaru et al., 2014). On top of the basal Ca activity, which was observed in control slices (Figures 7Ab), preincubation in cholesterol added more Ca transients (Figures 7Ac and 7B). Although the amplitude of Ca transients and Ca-increase area within the astrocytic arbor were similar between the cholesterol-incubated and control slices (Figures 7C and 7D), Ca increased loci within the cholesterol incubated astrocytes were closer to the cell body than the control; in other words, cholesterol induced Ca transients only in the central parts but not in peripheral regions within astrocytes

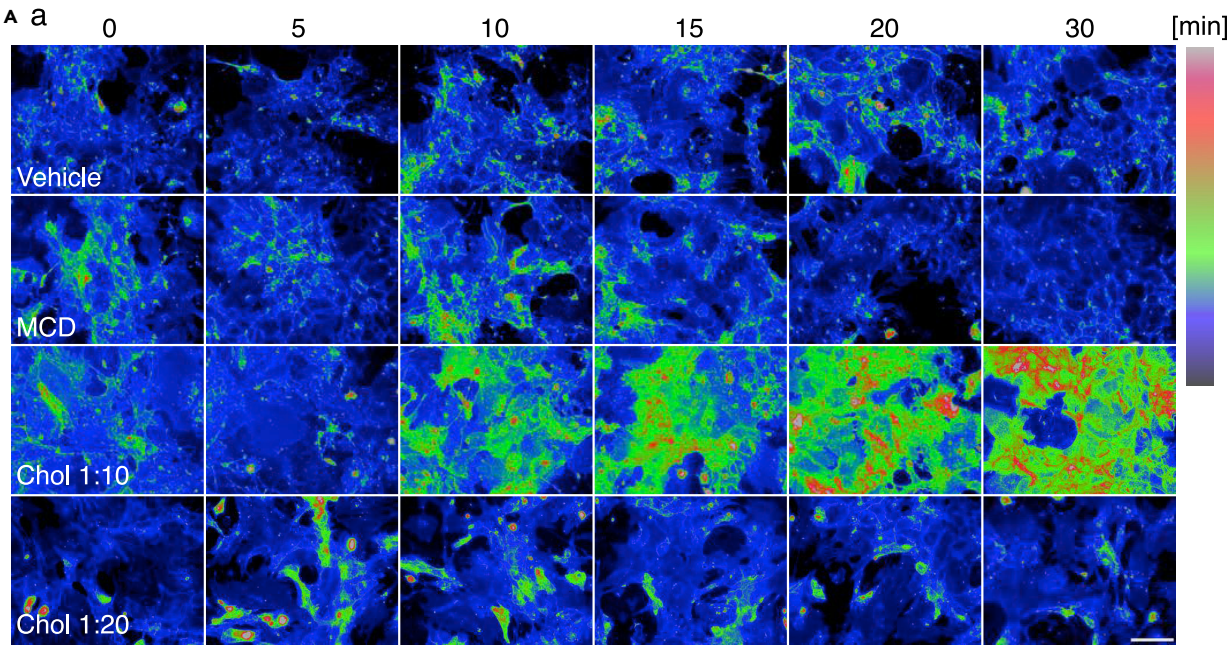

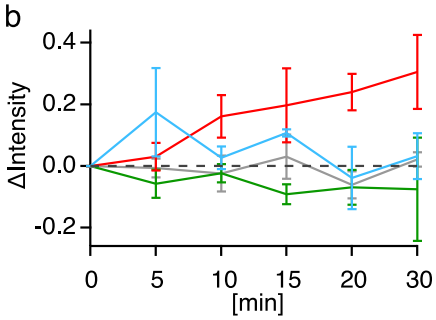

Vehicle
Cholesterol 1:10
MCD
Cholesterol 1:20

	5 min	10 min	15 min	20 min	30 min
Vehicle	ns	*	ns	**	*
MCD	ns	*	*	**	p = 0.06
Chol 1:20	ns	p = 0.07	ns	*	*

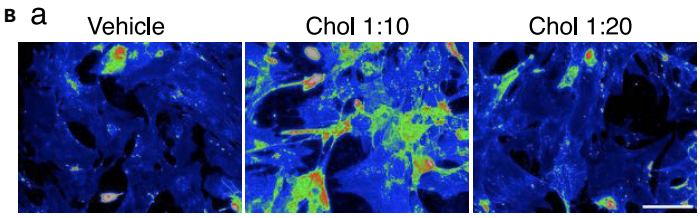

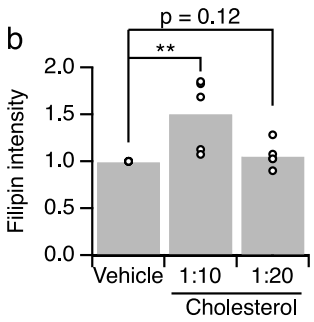

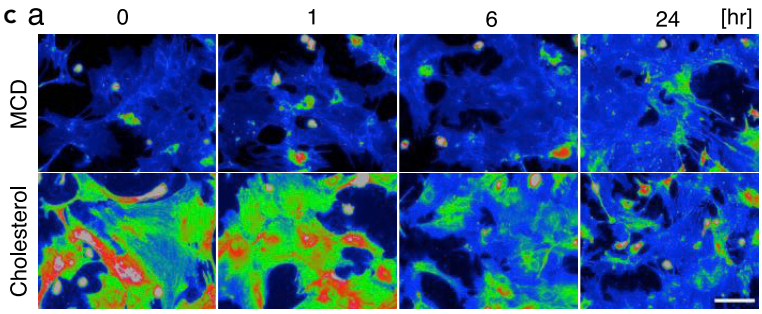

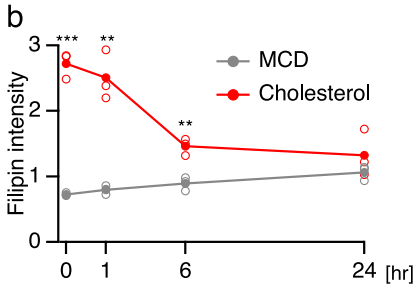

Figure 5. Accumulation of cholesterol in plasma membrane by extracellularly applied cholesterol

(A) Time-lapse images of plasma membrane cholesterol levels reported by the filipin dye (a). Time course changes of the filipin signal normalized to time 0 when reagents were applied (b). Scale bar, 100 μm. Number of samples were 3 for each trial. Table indicates statistical results between cholesterol 1:10 and other reagents (*p<0.05, **p<0.01, two-way repeated measures ANOVA and post hoc Steel-Dwass test).

(B) Filipin images after 24 h incubation in vehicle, cholesterol:MCD 1:10 and 1:20 (a) and quantification normalized by vehicle-treated control (b, n = 5). **p<0.01, Mann-Whitney U test. Scale bar, 100 μm.

(C) Time course of filipin signal after washout of MCD alone or cholesterol after 30 min incubation (a). Filipin intensity was quantified and normalized by that of vehicle-treated control (b, n = 3, **p<0.01, ***p<0.001, two-way repeated measures ANOVA and post-hoc Steel-Dwass test). Scale bar, 100 μm.

(Figure 7E). These results suggest that astrocytes in the brain may respond to extracellular cholesterol increase by Ca transients.

Blockage of cholesterol-induced Ca oscillation reduces viability of astrocytes

We examined whether extracellular cholesterol affects viability of astrocyte by staining with a dead cell marker, Ethidium Homodimer III (EthD-III) (Overmeyer et al., 2008), and an apoptosis marker, annexin-V. Since MCD without cholesterol reduced the viability of astrocytes, as mentioned above, vehicle (water) was used as a control. After 24 h incubation, EthD-III positive dead cells accounted for less than 10% of total astrocytes in the control vehicle medium and 25 μM cholesterol, and the rate increased to 30% under 250 μM cholesterol (Figures 8Aa and 8Ab), whereas 1:20 cholesterol/MCD did not alter EthD-III positive cell rate or cell density (Figure S6). When 2-APB (10 μM) was added to the cholesterol incubation, the EthD-III-positive cell rate remarkably increased with the high cholesterol concentrations, 100 and 250 μM. 2-APB itself did not have an apparent effect on the cell death rate. On the other hand, the cholesterol and/or the additional 2-APB did not obviously affect the ratio of annexin-V positive cells (Figure 8Ac), suggesting that the astrocyte death caused by the high concentrations of extracellular cholesterol and additional 2-APB was not because of apoptosis. Cell density, another index of viability, was decreased under 100 and 250 μM cholesterol incubation, which was accelerated by the addition of 2-APB (Figure 8Ad). The finding that 2-APB enhanced the deteriorating effect of cholesterol on astrocytes implies that Ca oscillation, which should have been blocked under 2-APB, may have an ameliorating effect on the survival of astrocytes under high extracellular cholesterol concentration.

The expression of GFAP in astrocytes is known to be promoted under stress conditions, including trauma and ischemia in the brain (Eng and Ghirnikar, 1994), and activation of GFAP expression was reported in cultured astrocytes after incubation in 50 μM cholesterol with ethanol as solvent for 48 h (Avila-Muñoz and Arias, 2015). Immunohistochemistry showed stronger GFAP signals in astrocytes treated with 250 μM cholesterol conjugated with MCD for 48 h in accordance with the previous report, without noticeable morphological changes compared to control astrocytes that were incubated with vehicle (Figure 8Ba). RT-PCR revealed an apparent increase in *gfap* transcripts in astrocytes treated with 50 μM ethanol dissolved- and 250 μM MCD-conjugated-cholesterol for 48 h, but not in those incubated for 24 h (Figure 8Bb). Compared to the rise time of GFAP protein expression (12 h) reported for cocaine or lipopolysaccharide (LPS) stimulation (Brahmachari et al., 2006; Yang et al., 2016), the increase in GFAP transcription under extracellular cholesterol took much longer time (48 h).

Ca oscillation plays a role in lipid droplet accumulation in astrocytes under high extracellular cholesterol

Cells store excess cholesterol in lipid droplets (Ikonen, 2008). Astrocytes remarkably increased the number of lipid droplets under excess extracellular cholesterol within 24 h (Figure 9). The intensity of Nile red, a lipid droplet marker, increased according to cholesterol concentration, and discernible bright dots, namely lipid droplets, appeared with 100 and 250 μM cholesterol (Figures 9Aa and 9Ab). When extracellular cholesterol was washed after 30 min incubation with 250 μM cholesterol, apparent lipid droplet formation appeared 6 h after the wash, which decreased to the baseline level at 24 h (Figure S7). When 2-APB, which blocks Ca oscillation, was added to the cholesterol incubation, lipid droplets became inconspicuous, but the overall Nile red signal tended to become even stronger, with the lipid droplet size affected especially in 25 μM cholesterol (Figure 9). Although the comparisons of the lipid droplet size between the 2-APB-incubated and DMSO control groups indicate statistical significances in the 25, 100 and 250 μM cholesterol conditions, the overall size distribution patterns of the two groups in 100 and 250 μM cholesterol look similar (Figure 9Bc). We consider that the lipid droplet size was not essentially affected by the 2-APB treatment in 100 and 250 μM cholesterol, but the statistics flagged them because of the large number of lipid droplets

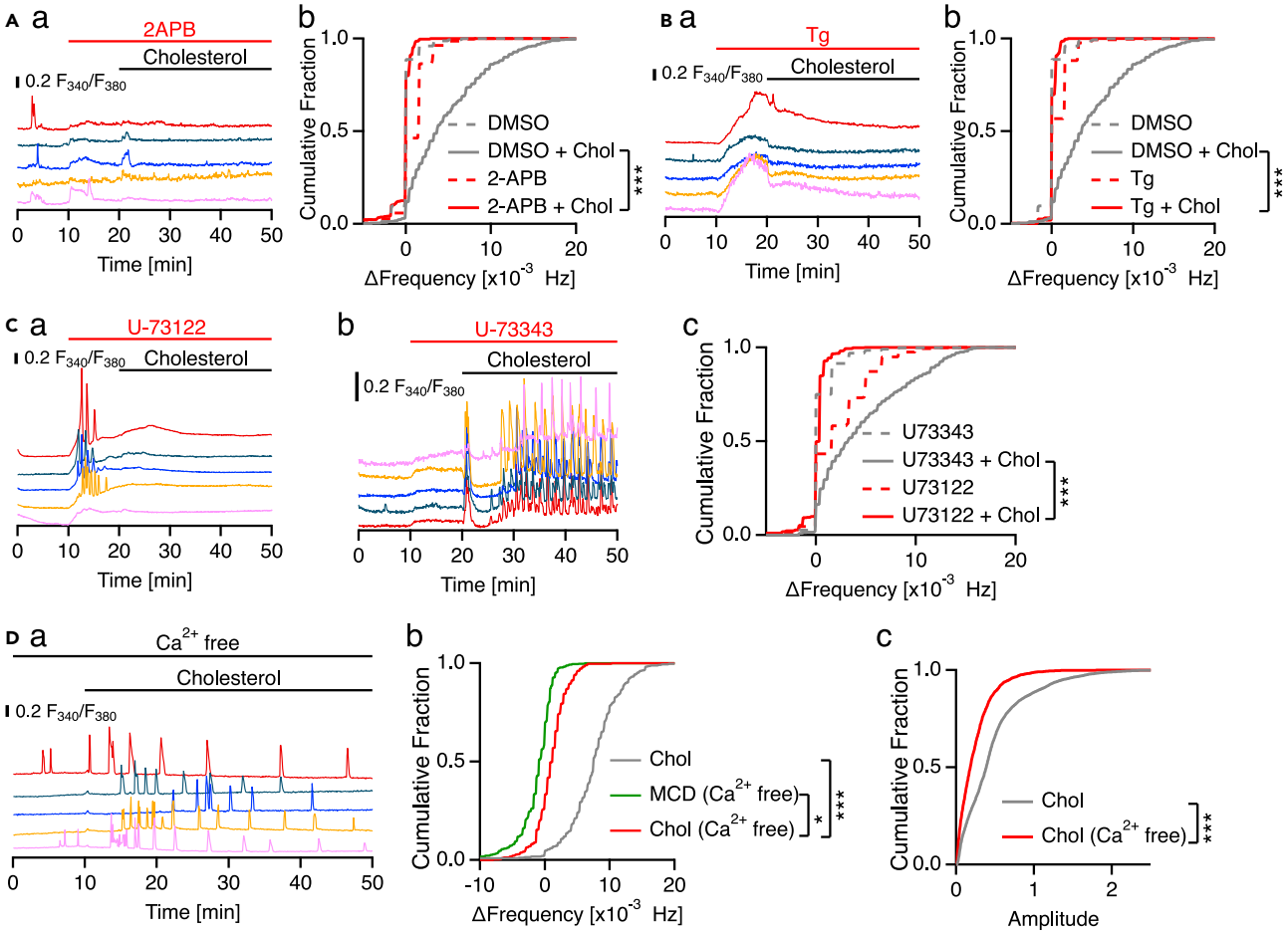

Figure 6. Cholesterol-induced Ca oscillation requires the PLC-IP$_3$ pathway

(A and B) Time course of Ca changes in astrocytes incubated with 2-APB (A) and thapsigargin (Tg, B) followed by cholesterol application (a) and cumulative fraction of ΔFrequency with DMSO control (b). ***p<0.001, Kruskal-Wallis test and post hoc Bonferroni corrected Mann-Whitney U test.

(C) Ca changes in U-73122 treated astrocytes (a) and ΔFrequency with a control group treated with an inactive analogue, U-73343 (b). ***p<0.001, Kruskal-Wallis test and post hoc Bonferroni corrected Mann-Whitney U test.

(D) Ca changes in cholesterol stimulated astrocytes in Ca free medium (a). ΔFrequency and amplitude are compared to the cholesterol (with Ca) group (b and c, the same data shown in Figure 2A) and to an MCD (Ca-free) group (b). *p<0.05, ***p<0.001, Kruskal-Wallis test and post hoc Bonferroni corrected Mann-Whitney U test. Number of cells(number of cultures): DMSO, 567(6); 2-APB, 359(5); Tg, 344(5); U-7312, 428(5); U-73343, 433(5); cholesterol (Cafree), 378(5); MCD (Cafree), 428(5).

to be compared (see the legend to Figure 9). These results suggest that Ca oscillation may play an important role in lipid droplet formation in astrocytes in excess cholesterol conditions.

DISCUSSION

In this study, we revealed that extracellular cholesterol application induces robust Ca oscillation only in astrocytes and that the cholesterol-induced Ca oscillation may be required for the survival of astrocytes under extracellular high cholesterol stress. Because the cholesterol-induced Ca oscillation lasted even after extracellular cholesterol washout and the rise time of cholesterol content in plasma membrane was close to the lag of Ca oscillation start, we consider that the cholesterol-induced Ca oscillation is triggered by the increase in cholesterol embedded in the plasma membrane. Our results further imply that the cholesterol-induced Ca oscillation may be required for the survival of astrocytes in a high-cholesterol environment by properly handling internalized cholesterol by storing them as lipid droplets.

The fact that cholesterol-induced Ca oscillation requires activation of the PLC-IP$_3$ receptor pathway suggests that accumulated cholesterol in the plasma membrane may activate plasma membrane-resident

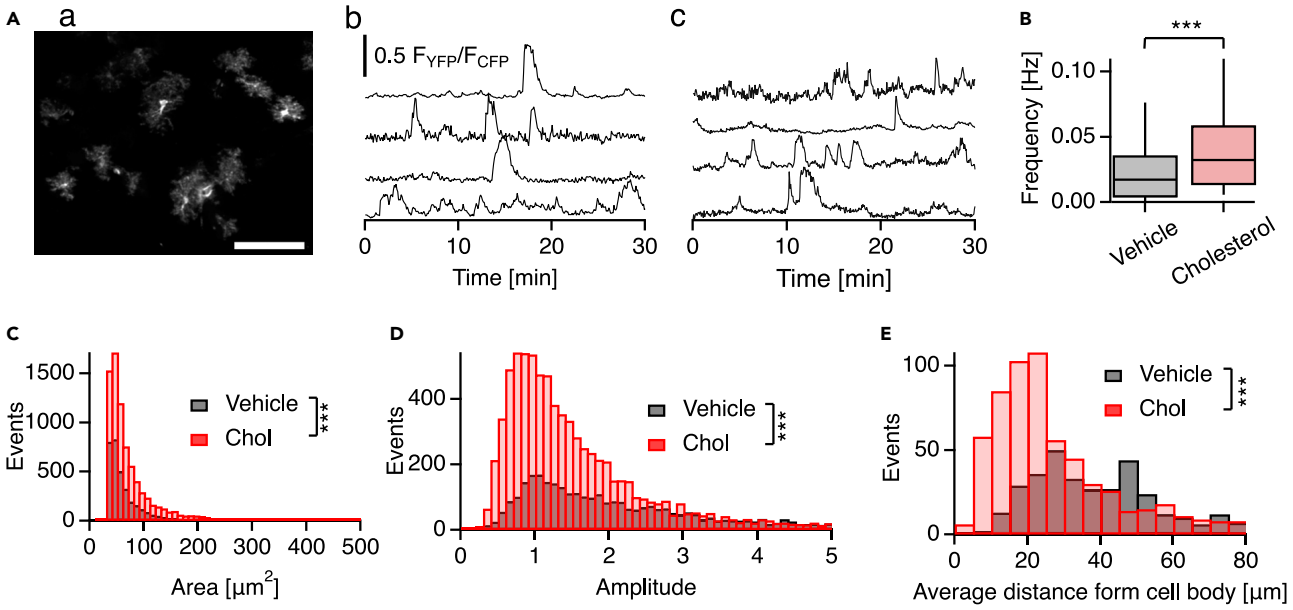

Figure 7. Cholesterol raises frequency of Ca events in astrocytes in hippocampal slice

(A) YC-Nano50 expressing astrocytes in dentate gyrus in a hippocampal slice (a) and typical traces from vehicle-incubated control (b) and cholesterol-incubated (c) astrocytes. Scale bar, 100 μm.

(B) Ca transient frequency of vehicle- and cholesterol-treated astrocytes. ***p<0.001, Mann-Whitney U test.

(C–E) Distribution of Ca-increase area within astrocytic arbor (C), amplitude of Ca event (D), and distance between Ca-increase locus and cell body (E). ***p<0.001, Mann-Whitney U test. Number of cells(number of slices/number of mice): cholesterol, 85(8/3), vehicle, 67(6/3).

receptors that activate PLC, such as GPCRs and receptor tyrosine kinases. The notion that several GPCRs and receptor tyrosine kinases have cholesterol-binding domains (Gimpl, 2016; Paila and Chattopadhyay, 2010) supports this idea. Furthermore, it was reported that cholesterol application increases PLC expression in the plasma membrane within 30 min (Chun et al., 2013). It is tempting to elucidate the molecular mechanism that transduces cholesterol load in the plasma membrane to the PLC activity and leads to Ca oscillation in astrocytes. Our data imply that smoothened, which possesses cholesterol-binding domains and is activated by cholesterol (Deshpande et al., 2019; Huang et al., 2016a; Luchetti et al., 2016), is not the sole candidate for the membrane receptors responsible to the cholesterol-induced Ca oscillation in astrocytes because there are differences in Ca response properties, such as Ca response kinetics and participation of gap junction. The fact that the cholesterol-induced Ca oscillation was not observed in neurons (Figure 1) and numbers of cell lines including the glioma-derived C6 cell line (Figure S2) but only in astrocytes implies that the putative plasma membrane receptor(s) that detects cholesterol increase in the plasma membrane may be expressed selectively in astrocytes. And the difference in the properties of cholesterol-induced Ca oscillation among astrocytes from hippocampus, cortex and spinal cord (Figures 2 and S4) may also reflect differences in the expression level of the putative cholesterol-sensitive receptor and/or its downstream signaling elements, as the heterogeneity of astrocytes among brain regions and even in the same region is obvious (Batiuk et al., 2020).

In this study, we revealed that blockade of cholesterol-induced Ca oscillation exacerbated astrocytic death under high cholesterol load. Although cholesterol-induced apoptotic cell death has been reported in vascular smooth muscle cell, pancreatic ß cell, and the SH-SY5Y human neuroblastoma cell line (Huang et al., 2016b; Lu et al., 2011; Yin et al., 2000), the astrocytic death observed in this study was not apoptotic, as the apoptotic marker, annexin-V, was negative. However, it has been reported that cholesterol accumulation induces necroptosis, a regulated form of necrosis, in SH-SY5Y cells (Funakoshi et al., 2016). Detailed mechanisms that led to cell death observed in this study are intriguing. It is noteworthy that the two phenomena, lipid droplet formation and prevention of astrocytic death from cholesterol load, were both related to the cholesterol-induced Ca oscillation. It would be tempting to determine whether lipid droplet formation is correlated with the avoidance of cell death.

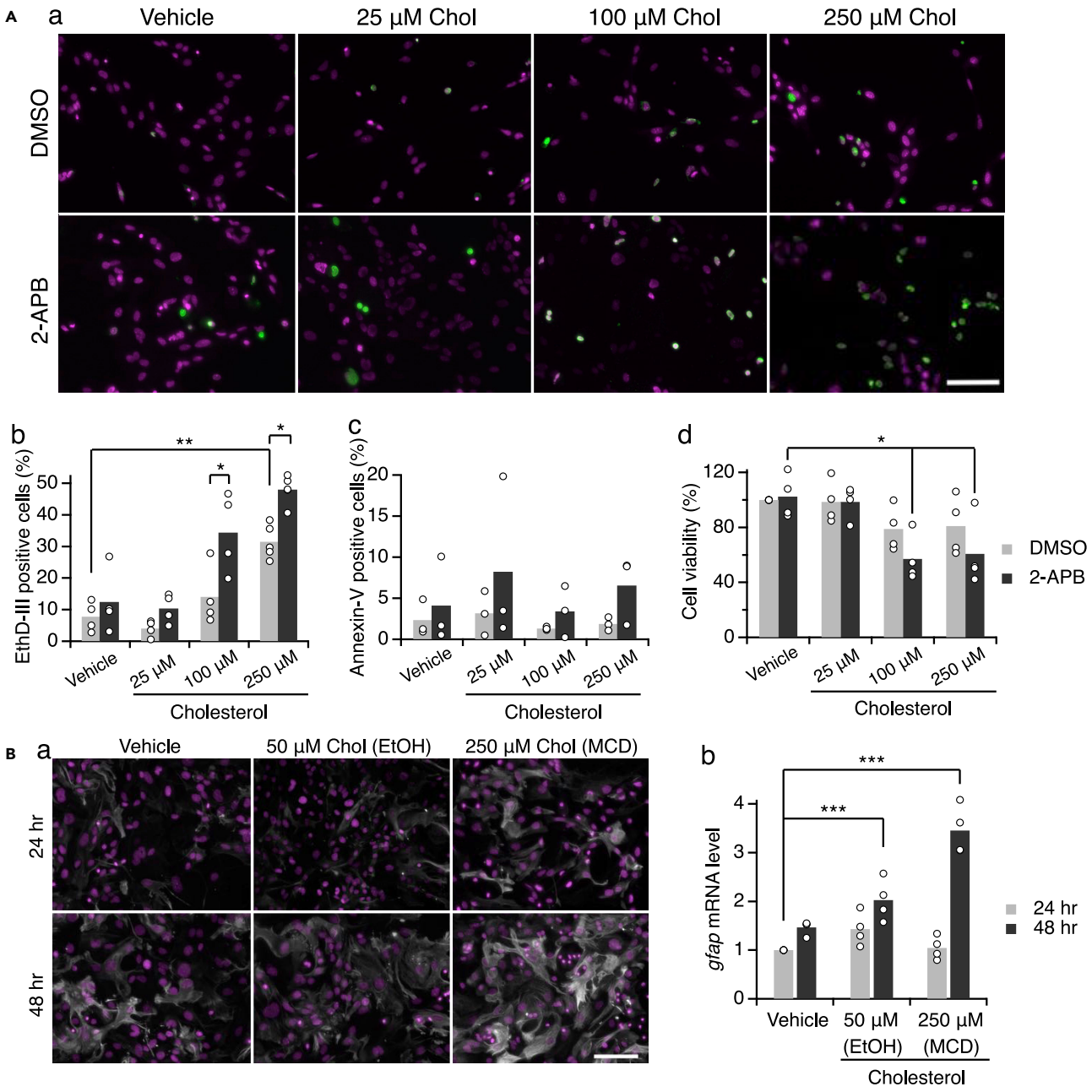

Figure 8. Cell death and GFAP expression induction in cholesterol treated astrocytes

(A) Cell viability assay after 24 h cholesterol incubation with 2-APB or DMSO as a vehicle control by staining with EthD-III (dead cell marker, green) and Hoechst (nuclear marker, magenta; a). Ab and c: proportion of EthD-III (b) and Annexin-V (p = 0.68, Kruskal-Wallis test; c) positive cells (black bars, 2-APB treatment; gray bars, DMSO treatment). Ad: cell density normalized by the vehicle control without 2-APB. Five independent experiment sets were performed.Scale bar, 100 μm *p<0.05, **p<0.001, Kruskal-Wallis test and post hoc Steel-Dwass test.

(B) Astrocytes stained with anti-GFAP antibody (white) and DAPI (magenta) after incubation with 250 μM cholesterol conjugated with MCD, 50 μM cholesterol dissolved in ethanol, and vehicle (addition of equivalent volume of water to the medium) for 24 and 48 h (a). Scale bar, 100 μm. Bb: relative *gfap* mRNA expression levels by real-time PCR (n = 4, respectively). ***p<0.001, Kruskal-Wallis test and post hoc Steel-Dwass test.

See also Figure S6.

Lipid droplets are organelles that store excess neutral lipids, such as triacylglycerol and sterol ester. Excess cholesterol in the cell is esterified by acyl-CoA: cholesterol O-acyltransferase (ACAT), and lipid droplet biogenesis occurs at the ER membrane (Olzmann and Carvalho, 2019). In this study, Nile red staining

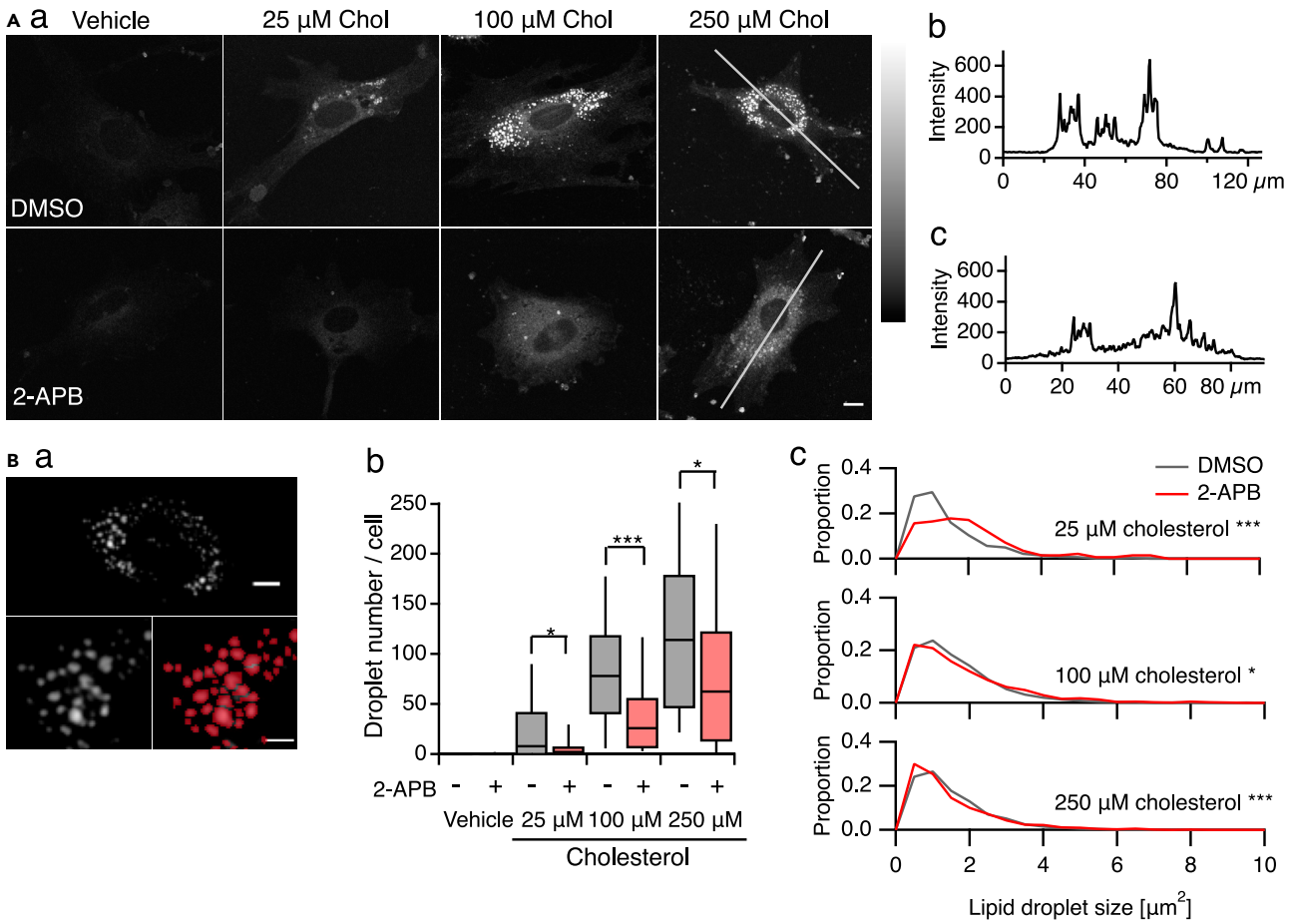

Figure 9. Lipid droplet formation and its inhibition by 2-APB in cholesterol-incubated astrocytes

(A) Typical Nile red staining patterns (a) and intensity distribution along lines with 250 μM cholesterol with DMSO (b) or with 2-APB (c) for 24 h. Scale bar, 10 μm.

(B and C) An example of lipid droplet detection by a watershed segmentation algorithm (a; see STAR Methods), number of droplets in astrocyte (b), and droplet size distribution (c). Red specks in (a) indicate detected lipid droplets. Scale bars: 20 μm (top), 10 μm (bottom). *p<0.05, ***p<0.001, Mann-Whitney U test. Total number of lipid droplets(number of cells, number of cultures): vehicle + DMSO, 6(23, 3); 25 μM cholesterol + DMSO, 725(40, 2); 100 μM cholesterol + DMSO, 275(42, 3); 250 μM cholesterol + DMSO, 4854(47, 3); vehicle + 2-APB, 1(25, 2); 25 μM cholesterol + 2-APB, 140(41, 3); 100 μM cholesterol + 2-APB, 1147(39, 3); 250 μM cholesterol + 2-APB, 2815(46, 3).

See also Figure S7.

revealed that droplet formation by cholesterol was depressed in 2-APB treated astrocytes; however, the signal level was rather increased with an even distribution pattern throughout the cytoplasm. Because Nile red stains neutral lipids, cholesterol per se is not stained; it must be esterified to be stained (Fowler and Greenspan, 1985). Thus, the cholesterol-induced Ca oscillation may play a role in lipid droplet biogenesis and possibly in cholesterol esterification. Phospholipase D1 (PLD1) is reported to be necessary for lipid droplet biogenesis and is located downstream of the extracellular signal-regulated kinase (ERK) signaling pathway (Andersson et al., 2006; Marchesan et al., 2003). It has been reported that the activities of ERK and an ERK activator, Ras, are positively regulated by the Ca oscillation frequency in HeLa cells (Kupzig et al., 2005). It is possible that the cholesterol-induced Ca oscillation promotes lipid droplet biogenesis through activation of the Ras-ERK signal, together with different scenarios that involve a variety of Ca-activated enzymes, including calcineurin, calpain, and Ca^{2+}/calmodulin-dependent protein kinases (Bagur and Hajnóczky, 2017), and downstream factors, such as nuclear factor of activated T-cells (NFAT), NF-κB, and c-jun N-terminal kinase (JNK) (Crabtree, 1999; Dolmetsch et al., 1997, 1998).

Under physiological conditions, extracellular cholesterol is conveyed by apolipoprotein, and the lipoprotein-cholesterol complex is captured by low-density lipoprotein (LDL) receptor families on the plasma

membrane and taken up by endocytosis. In this study, we used cholesterol/MCD complex instead of lipoprotein-cholesterol complex, and we confirmed that the cholesterol content in astrocytes was increased by cholesterol quantification (Figure 2M) and filipin staining (Figure 5). Therefore, cholesterol may have been taken up by astrocytes through a different mechanism from that for lipoprotein-cholesterol complex uptake. Free cholesterol transfer from low- and high-density lipoproteins to the plasma membrane has been reported in several cell types (Fong and Angel, 1989; Wüstner et al., 2004; Axmann et al., 2019). Under an LDL overload condition where cholesterol content in aortic smooth muscle cells approximately doubled, the route of 40% of the increased cholesterol was estimated to be via free cholesterol transfer to the cell surface (Slotte et al., 1988). It is likely that free cholesterol transfer from lipoproteins to plasma membrane may occur under high cholesterol conditions, which would induce Ca oscillation and subsequent events in astrocytes in the brain as observed in this study.

The 2- to 3-fold increase in free cholesterol content by incubation with 250 μM cholesterol (Figure 2M) overlaps with the free cholesterol content ranges reported in pathological conditions: about 1.5-fold higher cholesterol content in brain tissues of a hypercholesterolemia model mouse (Paul and Borah, 2017) and 1.5- to 3-fold higher accumulation of unesterified free cholesterol in a Niemann-Pick disease type C model fibroblasts (Newton et al., 2020; Xu et al., 2012). Thus, the cholesterol increase by incubation with cholesterol observed in this study could be relevant to pathological conditions.

Intracellular Ca increase has potential to produce reactive oxygen species (ROS) (Reynolds and Hastings, 1995; Tauffenberger and Magistretti, 2021), and cholesterol is susceptible to oxidation reactions to be transformed to oxysterols (Murphy and Johnson, 2008). Both ROS and oxysterols are reactive and influence variety of signaling pathways. It would be possible that the cholesterol-induced Ca oscillation activated ROS production, and the increased ROS, together with oxysterols converted from cholesterol by ROS, played some roles in the phenomena observed in this study, namely long-lasting Ca oscillation and lipid droplet formation. Further studies would be awaited.

The involvement of cholesterol in neurodegenerative diseases has been demonstrated. In Alzheimer's disease (AD), amyloid β (Aβ) production is reported to be promoted by increased membrane cholesterol in both neurons and astrocytes (Avila-Muñoz and Arias, 2015; Wang et al., 2021), and AD-related proteins such as amyloid precursor protein (APP), Aβ, and β-site APP cleaving enzyme 1 (BACE-1) are highly expressed in hypercholesterolemic model brains (Chen et al., 2016; Refolo et al., 2000; Thirumangalakudi et al., 2008), which was ameliorated by statin, a cholesterol biosynthesis blocker (DeKosky, 2005; Langness et al., 2020). These results suggest that cholesterolemia can cause cholesterol accumulation in the brain, leading to the AD pathology. Also the blood concentration of 24-OHC, a cholesterol metabolite mainly produced in the brain, is increased in patients of AD and multiple sclerosis (Lütjohann et al., 2000; Zhornitsky et al., 2016), suggesting that excess extracellular free cholesterol conditions may exist in pathological brains because of demyelination or neuronal death. Taking these lines of evidence into consideration, it would be intriguing to imagine that astrocytes under neurodegenerative diseases especially accompanying demyelination may be exposed to high extracellular cholesterol, and thus, the astrocytic reactions to cholesterol load revealed in this study, that is Ca oscillation leading to survival of astrocytes possibly through uptake and storage of cholesterol as lipid droplets, are taking place as an early step in the etiology. Further studies that link the cholesterol-induced events in astrocytes revealed in this study and neurodegenerative diseases are awaited.

Limitation of the study

In this study, we revealed that extracellularly applied cholesterol induces strong Ca oscillation in astrocytes, however two major questions remain. The first one is the identity of the receptor to cholesterol. It can be narrowed down to receptor(s) that activate PLC. Receptor screening is needed as a next step. The second question is whether the cholesterol-induced Ca oscillation observed in cultured astrocyte actually occurs in astrocytes in physiological and pathological brains. In this study, cholesterol was fed to cells by cholesterol/MCD complex which is not a natural composition but possesses high capacity for providing cholesterol in aqueous environment. Because the cholesterol content in the myelin in the brain is very high, extracellular cholesterol content in brain parenchyma could be raised very high on demyelination. Future works should examine whether astrocytes in the brain exhibit robust Ca oscillation because of extracellular cholesterol load on demyelination.

STAR★METHODS

Detailed methods are provided in the online version of this paper and include the following:

- KEY RESOURCES TABLE
- RESOURCE AVAILABILITY
  - Lead contact
  - Materials availability
  - Data and code availability
- EXPERIMENTAL MODEL AND SUBJECT DETAILS
  - Animals
  - Primary cell cultures and cell lines
- METHOD DETAILS
  - Reagents
  - Cell culture
  - Immunohistochemistry
  - Filipin staining
  - Cell culture imaging
  - Gene transfection and YC3.60 imaging
  - Cholesterol quantification
  - Real-time PCR
  - Cell viability assay
  - Ca imaging in brain slice
  - Lipid droplet staining
- QUANTIFICATION AND STATISTICAL ANALYSIS

SUPPLEMENTAL INFORMATION

Supplemental information can be found online at https://doi.org/10.1016/j.isci.2022.105138.

ACKNOWLEDGMENTS

We thank Drs. K. F. Tanaka and A. Natsubori for providing Mlc1-YC Nano50 mice, and Dr. A. Miyawaki for providing plasmid encoding YC3.60. This work was supported by Waseda University Grants for Special Research Projects (C.A.: 2020C-644, 2021E-023, 2021C-559; T.I.: 2019C-715, 2020C-778, 2021C-733).

AUTHOR CONTRIBUTIONS

Conceptualization, C.A. and T.I.; Methodology, C.A. and T.I.; Software, T.I.; Validation, C.A. and T.I; Formal Analysis, C.A. and T.I.; Investigation, C.A. and S.O.; Data Curation, C.A.; Writing – Original Draft, C.A. and T.I.; Writing – Review and Editing, C.A. and T.I.; Visualization, C.A.; Supervision, T.I.; Project Administration, T.I.; Funding Acquisition, C.A. and T.I.

DECLARATION OF INTERESTS

The authors declare no competing interests.

Received: March 25, 2022
Revised: August 8, 2022
Accepted: September 10, 2022
Published: October 21, 2022

REFERENCES

Adachi, C., Kakinuma, N., Jo, S.H., Ishii, T., Arai, Y., Arai, S., Kitaguchi, T., Takeda, S., and Inoue, T. (2019). Sonic hedgehog enhances calcium oscillations in hippocampal astrocytes. J. Biol. Chem. *294*, 16034–16048. https://doi.org/10.1074/jbc.RA119.007883.

Andersson, L., Boström, P., Ericson, J., Rutberg, M., Magnusson, B., Marchesan, D., Ruiz, M., Asp, L., Huang, P., Frohman, M.A., et al. (2006). PLD1 and ERK2 regulate cytosolic lipid droplet formation. J. Cell Sci. *119*, 2246–2257. https://doi.org/10.1242/jcs.02941.

Avila-Muñoz, E., and Arias, C. (2015). Cholesterol-induced astrocyte activation is associated with increased amyloid precursor protein expression and processing. Glia *63*, 2010–2022. https://doi.org/10.1002/glia.22874.

Axmann, M., Strobl, W.M., Plochberger, B., and Stangl, H. (2019). Cholesterol transfer at the plasma membrane. Atherosclerosis *290*, 111–117. https://doi.org/10.1016/j.atherosclerosis.2019.09.022.

Baek, S.-J., Park, A., Ahn, Y.-J., and Choo, J. (2015). Baseline correction using asymmetrically reweighted penalized least squares smoothing.

Analyst *140*, 250–257. https://doi.org/10.1039/C4AN01061B.

Bagur, R., and Hajnóczky, G. (2017). Intracellular Ca^{2+}sensing: its role in calcium homeostasis and signaling. Mol. Cell *66*, 780–788. https://doi.org/10.1016/j.molcel.2017.05.028.

Batiuk, M.Y., Martirosyan, A., Wahis, J., de Vin, F., Marneffe, C., Kusserow, C., Koeppen, J., Viana, J.F., Oliveira, J.F., Voet, T., et al. (2020). Identification of region-specific astrocyte subtypes at single cell resolution. Nat. Commun. *11*, 1220. https://doi.org/10.1038/s41467-019-14198-8.

Brahmachari, S., Fung, Y.K., and Pahan, K. (2006). Induction of glial fibrillary acidic protein expression in astrocytes by Nitric Oxide. J. Neurosci. *26*, 4930–4939. https://doi.org/10.1523/JNEUROSCI.5480-05.2006.

Brennan, D., Chen, X., Cheng, L., Mahoney, M., and Riobo, N.A. (2012). Noncanonical hedgehog signaling. Vitam. Horm. *88*, 55–72. https://doi.org/10.1016/B978-0-12-394622-5.00003-1.

Cannarozzo, C., Fred, S.M., Girych, M., Biojone, C., Enkavi, G., Róg, T., Vattulainen, I., Casarotto, P.C., and Castrén, E. (2021). Cholesterol-recognition motifs in the transmembrane domain of the tyrosine kinase receptor family: the case of TRKB. Eur. J. Neurosci. *53*, 3311–3322. https://doi.org/10.1111/ejn.15218.

Chen, Y.L., Wang, L.M., Chen, Y., Gao, J.Y., Marshall, C., Cai, Z.Y., Hu, G., and Xiao, M. (2016). Changes in astrocyte functional markers and β-amyloid metabolism-related proteins in the early stages of hypercholesterolemia. Neuroscience *316*, 178–191. https://doi.org/10.1016/j.neuroscience.2015.12.039.

Chun, Y.S., Oh, H.G., Park, M.K., Kim, T.-W., and Chung, S. (2013). Increasing membrane cholesterol level increases the Amyloidogenic peptide by enhancing the expression of phospholipase C. J. Neurodegener. Dis. *2013*, 407903. https://doi.org/10.1155/2013/407903.

Crabtree, G.R. (1999). Generic signals and specific outcomes: signaling through Ca^{2+}, calcineurin, and NF-AT. Cell *96*, 611–614. https://doi.org/10.1016/S0092-8674(00)80571-1.

DeKosky, S.T. (2005). Statin therapy in the treatment of Alzheimer disease: what is the rationale? Am. J. Med. *118*, 48–53. https://doi.org/10.1016/j.amjmed.2005.09.006.

Deshpande, I., Liang, J., Hedeen, D., Roberts, K.J., Zhang, Y., Ha, B., Latorraca, N.R., Faust, B., Dror, R.O., Beachy, P.A., et al. (2019). Smoothened stimulation by membrane sterols drives Hedgehog pathway activity. Nature *571*, 284–288. https://doi.org/10.1038/s41586-019-1355-4.

Dolmetsch, R.E., Lewis, R.S., Goodnow, C.C., and Healy, J.I. (1997). Differential activation of transcription factors induced by Ca^{2+} response amplitude and duration. Nature *386*, 855–858. https://doi.org/10.1038/386855a0.

Dolmetsch, R.E., Xu, K., and Lewis, R.S. (1998). Calcium oscillations increase the efficiency and specificity of gene expression. Nature *392*, 933–936. https://doi.org/10.1038/31960.

Dorris, D.M., Hauser, C.A., Minnehan, C.E., and Meitzen, J. (2014). An aerator for brain slice experiments in individual cell culture plate wells. J. Neurosci. Methods *238*, 1–10. https://doi.org/10.1016/j.jneumeth.2014.09.017.

Eng, L.F., and Ghirnikar, R.S. (1994). GFAP and astrogliosis. Brain Pathol *4*, 229–237. https://doi.org/10.1111/j.1750-3639.1994.tb00838.x.

Fong, B.S., and Angel, A. (1989). Transfer of free and esterified cholesterol from low-density lipoproteins and high-density lipoproteins to human adipocytes. Biochim. Biophys. Acta *1004*, 53–60. https://doi.org/10.1016/0005-2760(89)90212-9.

Fowler, S.D., and Greenspan, P. (1985). Application of Nile red, a fluorescent hydrophobic probe, for the detection of neutral lipid deposits in tissue sections: comparison with oil red O. J. Histochem. Cytochem. *33*, 833–836. https://doi.org/10.1177/33.8.4020099.

Funakoshi, T., Aki, T., Tajiri, M., Unuma, K., and Uemura, K. (2016). Necroptosis-like neuronal cell death caused by cellular cholesterol accumulation. J. Biol. Chem. *291*, 25050–25065. https://doi.org/10.1074/jbc.M116.727404.

Galland, F., Seady, M., Taday, J., Smaili, S.S., Gonçalves, C.A., and Leite, M.C. (2019). Astrocyte culture models: molecular and function characterization of primary culture, immortalized astrocytes and C6 glioma cells. Neurochem. Int. *131*, 104538. https://doi.org/10.1016/j.neuint.2019.104538.

Gimpl, G. (2016). Interaction of G protein coupled receptors and cholesterol. Chem. Phys. Lipids *199*, 61–73. https://doi.org/10.1016/j.chemphyslip.2016.04.006.

Huang, P., Nedelcu, D., Watanabe, M., Jao, C., Kim, Y., Liu, J., and Salic, A. (2016a). Cellular cholesterol directly activates smoothened in hedgehog signaling. Cell *166*, 1176–1187.e14. https://doi.org/10.1016/j.cell.2016.08.003.

Huang, Y.N., Lin, C.I., Liao, H., Liu, C.Y., Chen, Y.H., Chiu, W.C., and Lin, S.H. (2016b). Cholesterol overload induces apoptosis in SH-SY5Y human neuroblastoma cells through the up regulation of flotillin-2 in the lipid raft and the activation of BDNF/Trkb signaling. Neuroscience *328*, 201–209. https://doi.org/10.1016/j.neuroscience.2016.04.043.

Ihaka, R., and Gentleman, R. (1996). R: aLanguage for data analysis and graphics. J. Comput. Graph Stat. *5*, 299–314. https://doi.org/10.2307/1390807.

Ikonen, E. (2008). Cellular cholesterol trafficking and compartmentalization. Nat. Rev. Mol. Cell Biol. *9*, 125–138. https://doi.org/10.1038/nrm2336.

Inoue, T. (2018). TI Workbench, an integrated software package for electrophysiology and imaging. Microscopy *67*, 129–143. https://doi.org/10.1093/jmicro/dfy015.

Jenkins, D. (2009). Hedgehog signalling: emerging evidence for non-canonical pathways. Cell. Signal. *21*, 1023–1034. https://doi.org/10.1016/j.cellsig.2009.01.033.

Kanemaru, K., Sekiya, H., Xu, M., Satoh, K., Kitajima, N., Yoshida, K., Okubo, Y., Sasaki, T., Moritoh, S., Hasuwa, H., et al. (2014). In vivo visualization of subtle, transient, and local activity of astrocytes using an ultrasensitive Ca^{2+}indicator. Cell Rep. *8*, 311–318. https://doi.org/10.1016/j.celrep.2014.05.056.

Kupzig, S., Walker, S.A., and Cullen, P.J. (2005). The frequencies of calcium oscillations are optimized for efficient calcium-mediated activation of Ras and the ERK/MAPK cascade. Proc. Natl. Acad. Sci. USA *102*, 7577–7582. https://doi.org/10.1073/pnas.0409611102.

Lange, S.C., Bak, L.K., Waagepetersen, H.S., Schousboe, A., and Norenberg, M.D. (2012). Primary cultures of astrocytes: their value in understanding astrocytes in health and disease. Neurochem. Res. *37*, 2569–2588. https://doi.org/10.1007/s11064-012-0868-0.

Langness, V.F., van der Kant, R., Das, U., Wang, L., Chaves, R., Dos, S., and Goldstein, L.S.B. (2020). Cholesterol lowering drugs reduce APP processing to Aβ by inducing APP dimerization. Mol. Biol. Cell *32*, 247–259. https://doi.org/10.1091/mbc.E20-05-0345.

Lingwood, D., and Simons, K. (2010). Lipid rafts as a membrane-organizing principle. Science *327*, 46–50. https://doi.org/10.1126/science.1174621.

Lu, X., Liu, J., Hou, F., Liu, Z., Cao, X., Seo, H., and Gao, B. (2011). Cholesterol induces pancreatic β cell apoptosis through oxidative stress pathway. Cell Stress Chaperones *16*, 539–548. https://doi.org/10.1007/s12192-011-0265-7.

Luchetti, G., Sircar, R., Kong, J.H., Nachtergaele, S., Sagner, A., Byrne, E.F., Covey, D.F., Siebold, C., and Rohatgi, R. (2016). Cholesterol activates the G-protein coupled receptor Smoothened to promote Hedgehog signaling. Elife *5*, e20304. https://doi.org/10.7554/eLife.20304.

Lütjohann, D., Papassotiropoulos, A., Björkhem, I., Locatelli, S., Bagli, M., Oehring, R.D., Schlegel, U., Jessen, F., Rao, M.L., von Bergmann, K., et al. (2000). Plasma 24S-hydroxycholesterol (cerebrosterol) is increased in Alzheimer and vascular demented patients. J. Lipid Res. *41*, 195–198.

Marchesan, D., Rutberg, M., Andersson, L., Asp, L., Larsson, T., Borén, J., Johansson, B.R., and Olofsson, S.-O. (2003). A phospholipase D-dependent process forms lipid droplets containing Caveolin, Adipocyte differentiation-related protein, and Vimentin in a cell-free system. J. Biol. Chem. *278*, 27293–27300. https://doi.org/10.1074/jbc.M301430200.

Murphy, R.C., and Johnson, K.M. (2008). Cholesterol, reactive oxygen species, and the formation of biologically active mediators. J. Biol. Chem. *283*, 15521–15525. https://doi.org/10.1074/jbc.R700049200.

Nagai, T., Yamada, S., Tominaga, T., Ichikawa, M., and Miyawaki, A. (2004). Expanded dynamic range of fluorescent indicators for Ca^{2+} by circularly permuted yellow fluorescent proteins. Proc. Natl. Acad. Sci. USA *101*, 10554–10559. https://doi.org/10.1073/pnas.0400417101.

Newton, J., Palladino, E.N.D., Weigel, C., Maceyka, M., Gräler, M.H., Senkal, C.E., Enriz, R.D., Marvanova, P., Jampilek, J., Lima, S., et al.

(2020). Targeting defective sphingosine kinase 1 in Niemann-Pick type C disease with an activator mitigates cholesterol accumulation. J. Biol. Chem. *295*, 9121–9133. https://doi.org/10.1074/jbc.RA120.012659.

Norman, A.W., Demel, R.A., de Kruyff, B., and van Deenen, L.L.M. (1972). Studies on the biological properties of polyene antibiotics: evidence for the direct interaction offilipin with cholesterol. J. Biol. Chem. *247*, 1918–1929. https://doi.org/10.1016/S0021-9258(19)45558-0.

Olzmann, J.A., and Carvalho, P. (2019). Dynamics and functions of lipid droplets. Nat. Rev. Mol. Cell Biol. *20*, 137–155. https://doi.org/10.1038/s41580-018-0085-z.

Overmeyer, J.H., Kaul, A., Johnson, E.E., and Maltese, W.A. (2008). Active Ras triggers death in Glioblastoma cells through Hyperstimulation of Macropinocytosis. Mol. Cancer Res. *6*, 965–977. https://doi.org/10.1158/1541-7786.MCR-07-2036.

Paila, Y.D., and Chattopadhyay, A. (2010). Membrane cholesterol in the function and organization of G-protein coupled receptors. Subcell. Biochem. *51*, 439–466. https://doi.org/10.1007/978-90-481-8622-8_16.

Paul, R., and Borah, A. (2017). Global loss of acetylcholinesterase activity with mitochondrial complexes inhibition and inflammation in brain of hypercholesterolemic mice. Sci. Rep. *7*, 17922. https://doi.org/10.1038/s41598-017-17911-z.

Refolo, L.M., Pappolla, M.A., Malester, B., LaFrancois, J., Bryant-Thomas, T., Wang, R., Tint, G.S., Sambamurti, K., and Duff, K. (2000). hypercholesterolemia accelerates the alzheimer's amyloid pathology in a transgenic mouse model. Neurobiol. Dis. *7*, 321–331. https://doi.org/10.1006/nbdi.2000.0304.

Reynolds, I.J., and Hastings, T.G. (1995). Glutamate induces the production of reactive oxygen species in cultured forebrain neurons following NMDA receptor activation. J. Neurosci. *15*, 3318–3327. https://doi.org/10.1523/JNEUROSCI.15-05-03318.1995.

Richner, M., Jager, S.B., Siupka, P., and Vaegter, C.B. (2017). Hydraulic Extrusion of the Spinal Cord and Isolation of Dorsal Root Ganglia in Rodents. J. Vis. Exp. *55226*. https://doi.org/10.3791/55226.

Samios, V.N., and Inoue, T. (2014). Interleukin-1β and interleukin-6 affect electrophysiological properties of thalamic relay cells. Neurosci. Res. *87*, 16–25. https://doi.org/10.1016/j.neures.2014.06.011.

Slotte, J.P., Chait, A., and Bierman, E.L. (1988). Cholesterol accumulation in aortic smooth muscle cells exposed to low density lipoproteins. Contribution of free cholesterol transfer. Arteriosclerosis *8*, 750–758. https://doi.org/10.1161/01.ATV.8.6.750.

Tauffenberger, A., and Magistretti, P.J. (2021). Reactive oxygen species: beyond their reactive behavior. Neurochem. Res. *46*, 77–87. https://doi.org/10.1007/s11064-020-03208-7.

Thirumangalakudi, L., Prakasam, A., Zhang, R., Bimonte-Nelson, H., Sambamurti, K., Kindy, M.S., and Bhat, N.R. (2008). High cholesterol-induced neuroinflammation and amyloid precursor protein processing correlate with loss of working memory in mice. J. Neurochem. *106*, 475–485. https://doi.org/10.1111/j.1471-4159.2008.05415.x.

Vincent, L., and Soille, P. (1991). Watersheds in digital spaces: an efficient algorithm based on immersion simulations. IEEE Trans. Pattern Anal. Mach. Intell. *13*, 583–598. https://doi.org/10.1109/34.87344.

Wang, H., Kulas, J.A., Wang, C., Holtzman, D.M., Ferris, H.A., and Hansen, S.B. (2021). Regulation of beta-amyloid production in neurons by astrocyte-derived cholesterol. Proc. Natl. Acad. Sci. USA *118*. e2102191118. https://doi.org/10.1073/pnas.2102191118.

Wang, Y., DelRosso, N.V., Vaidyanathan, T.V., Cahill, M.K., Reitman, M.E., Pittolo, S., Mi, X., Yu, G., and Poskanzer, K.E. (2019). Accurate quantification of astrocyte and neurotransmitter fluorescence dynamics for single-cell and population-level physiology. Nat. Neurosci. *22*, 1936–1944. https://doi.org/10.1038/s41593-019-0492-2.

Wüstner, D., Mondal, M., Huang, A., and Maxfield, F.R. (2004). Different transport routes for high density lipoprotein and its associated free sterol in polarized hepatic cells. J. Lipid Res. *45*, 427–437. https://doi.org/10.1194/jlr.M300440-JLR200.

Xu, M., Liu, K., Swaroop, M., Porter, F.D., Sidhu, R., Firnkes, S., Finkes, S., Ory, D.S., Marugan, J.J., Xiao, J., et al. (2012). δ-Tocopherol reduces lipid accumulation in Niemann-Pick type C1 and Wolman cholesterol storage disorders. J. Biol. Chem. *287*, 39349–39360. https://doi.org/10.1074/jbc.M112.357707.

Yang, L., Yao, H., Chen, X., Cai, Y., Callen, S., and Buch, S. (2016). Role of Sigma receptor in cocaine-mediated induction of glial fibrillary acidic protein: Implications for HAND. Mol. Neurobiol. *53*, 1329–1342. https://doi.org/10.1007/s12035-015-9094-5.

Yin, J., Chaufour, X., McLachlan, C., McGuire, M., White, G., King, N., and Hambly, B. (2000). Apoptosis of vascular smooth muscle cells induced by cholesterol and its oxides in vitro and in vivo. Atherosclerosis *148*, 365–374. https://doi.org/10.1016/s0021-9150(99)00286-5.

Zhang, Y., and Barres, B.A. (2010). Astrocyte heterogeneity: an underappreciated topic in neurobiology. Curr. Opin. Neurobiol. *20*, 588–594. https://doi.org/10.1016/j.conb.2010.06.005.

Zhornitsky, S., McKay, K.A., Metz, L.M., Teunissen, C.E., and Rangachari, M. (2016). Cholesterol and markers of cholesterol turnover in multiple sclerosis: relationship with disease outcomes. Mult. Scler. Relat. Disord. *5*, 53–65. https://doi.org/10.1016/j.msard.2015.10.005.

Zidovetzki, R., and Levitan, I. (2007). Use of cyclodextrins to manipulate plasma membrane cholesterol content: evidence, misconceptions and control strategies. Biochim. Biophys. Acta *1768*, 1311–1324. https://doi.org/10.1016/j.bbamem.2007.03.026.

STAR★METHODS

KEY RESOURCES TABLE

REAGENT or RESOURCE	SOURCE	IDENTIFIER
Antibodies		
Mouse monoclonal anti-NeuN	Millipore	Cat# MAB377; RRID: AB_2298772
Goat polyclonal anti-GFAP	Abcam	Cat# ab53554; RRID: AB_880202
Rabbit polyclonal anti-Iba1	FUJIFILM Wako	Cat# 019–19741; RRID: AB_839504
Donkey anti-mouse IgG H&L (Alexa Fluor 594)	Abcam	Cat# ab150108; RRID: AB_2732073
Chicken anti-goat IgG (H + L) antibody, Alexa Fluor 488 conjugated	Molecular probes	Cat# A-21467, RRID: AB_141893
Donkey anti-Rabbit IgG (H + L) Highly cross-absorbed secondary antibody, Alexa Fluor 594	Thermo Fisher Scientific	Cat# A-21207; RRID: AB_141637
Chemicals, peptides, and recombinant proteins		
Cholesterol	Nacalai tesque	08721-62; CAS: 57-88-5
Methyl-ß-cyclodextrin	Sigma-Aldrich	332615; CAS: 128446-36-6
Tetrodotoxin	LATOXAN	L8503; CAS: 4368-28-9
2-APB	Tokyo Chemical Industry	D0281; CAS: 524-95-8
Thapsigargin	Nacalai tesque	33637-31; CAS: 67526-95-8
U-73122	Cayman chemical	70740; CAS: 112648-68-7
U-73343	Cayman chemical	17339; CAS: 142878-12-4
Carbenoxolone	Sigma-Aldrich	C4790; CAS: 7421-40-1
Fura 2-AM solution	Dojindo	343-05401; CAS: 108964-32-5
Nile red	Thermo Fisher Scientific	N-1142
Filipin	Sigma-Aldrich	F9765
Critical commercial assays		
Apoptotic/Necrotic/Healthy Cells Detection Kit	PromoCell	PK-CA707-30018
Amaxa Basic Nucleofector Kit for primary mammalian glial cells	Lonza	Cat# VPI-1006
ISOGEN II RNA extraction kit	NIPPON GENE	311-07361
THUNDERBIRD SYBR qPCR/RT kit	Toyobo	QPS201/FSQ101
Amplex™ Red Cholesterol Assay Kit	Invitrogen	A12216
Experimental models: Cell lines		
Rat: C6 cells	JCRB	Cat# IFO50110
African green monkey: COS-7 cells	N/A	N/A
Human: HEK293T cells	N/A	N/A
Human: HeLa cells	N/A	N/A
Mouse: NIH/3T3 cells	N/A	N/A
Experimental models: Organisms/strains		
Mouse: Slc:ICR	Japan SLC	N/A
Mouse: Mlc1-tTA::tetO-YC-Nano50	Kanemaru et al., 2014	N/A
Oligonucleotides		
Primer: mouse *gfap* forward: 5′-TTGCTGGAGGGCGAAGAAAA-3′	This paper	N/A
Primer: mouse *gfap* reverse: 5′-TGCTTTTGCCCCCTCGGAT-3′	This paper	N/A
Primer: *ß-actin* forward: 5′-GCTCCTAGCACCATGAAGA-3′	This paper	N/A
Primer: *ß-actin* reverse: 5′-ACTCCTGCTTGCTGATCCAC-3′	This paper	N/A

(*Continued on next page*)

Continued

REAGENT or RESOURCE	SOURCE	IDENTIFIER
Primer: genotyping tetOup: 5′-AGCAGAGCTCGTTTAGTGAACCGT-3′	Kanemaru et al., 2014	N/A
Primer: genotyping intronlow: 5′-AAGGCAGGATGATGACCAGGATGT-3′	Kanemaru et al., 2014	N/A
Primer: genotyping MlcU-657: 5′-AAATTCAGGAAGCTGTGTGCCTGC-3′	Kanemaru et al., 2014	N/A
Primer: genotyping mtTA24L: 5′-CGGAGTTGATCACCTTGGACTTGT-3′	Kanemaru et al., 2014	N/A
Recombinant DNA		
Plasmid: YC3.60	Nagai et al., 2004	N/A
Software and algorithms		
TI Workbench	Inoue, 2018	http://inouelab.biomed.sci.waseda.ac.jp/inouelab-web/tiwb.html
R (version 4.0.3)	Ihaka and Gentleman, 1996	https://www.r-project.org/
Igor Pro	WaveMetrics	http://www.wavemetrics.com/products/igorpro/igorpro.htm RRID:SCR_000325

RESOURCE AVAILABILITY

Lead contact

Further information and requests for resources and reagents should be directed to and will be fulfilled by the lead contact, Takafumi Inoue (inoue.t@waseda.jp).

Materials availability

This study did not generate new unique reagents.

Data and code availability

- All data reported in this article will be shared by the lead contact on request.
- This article does not report original code.
- Any additional information required to reanalyze the data reported in this article is available from the lead contact on request.

EXPERIMENTAL MODEL AND SUBJECT DETAILS

Animals

Female 4-8-week-old Mlc1-tTA:tetO-YC-Nano50 mice (Kanemaru et al., 2014) gifted from Dr. K. F. Tanaka (Keio University) were used in this study. Mice were housed under a constant ambient temperature and relative humidity. Less than five mice were housed per cage under a 12-h light/dark cycle and provided food and water *ad libitum*. Genotyping was conducted using the primer sets reported previously (see the key resources table). Animal care was in accordance with guidelines outlined by the Institutional Animal Care and Use Committee of Waseda University. The animal experiment protocol was approved by the Committee on the Ethics of Animal Experiments of Waseda University. All efforts were made to minimize the number of animals used and their suffering during experiments.

Primary cell cultures and cell lines

All primary cell cultures were prepared from embryonic day (E) 17 ICR mice purchased from Sankyo Labo Service Corporation (Tokyo, Japan). Primary hippocampal neuron-astrocyte co-culture was harvested in Neurobasal-A medium supplemented with NeuroBrew-21, L-glutamine and penicillin/streptomycin, and primary glial cultures were maintained in DMEM/Ham's F12 medium supplemented with 5% horse serum, 5% fetal bovine serum, L-glutamine and penicillin/streptomycin. All cell lines were cultured in DMEM medium supplemented with 10% fetal bovine serum and penicillin/streptomycin. All cell cultures were incubated at 37°C and 5% CO_2. No cell authentication was performed.

METHOD DETAILS

Reagents

Cholesterol (08721-62, Nacalai tesque, Kyoto, Japan)/methyl-β-cyclodextrin (MCD, 332615, Sigma-Aldrich, Tokyo, Japan) complex was prepared as described previously (Huang et al., 2016a) with the molar ratio of MCD to cholesterol 10:1 or 20:1. Briefly, 40 mM cholesterol in EtOH and 40 mM MCD in water were mixed 1:10 or 1:20, and evaporated under vacuum for 1-2 weeks. The dried complex was dissolved in water to set the cholesterol concentration at 2.5 mM and stored at 4°C. TTX (Latoxan Laboratory, Portes lès Valence, France) was dissolved in 12.7 mM citrate solution at 1 mM and stored at 4°C. 2-APB (D0281, Tokyo Chemical Industry, Tokyo, Japan) was dissolved in Dimethyl Sulfoxide (DMSO, D2650, Sigma-Aldrich) at 50 mM and stored at −20°C. Thapsigargin (Tg, 33637-31, Nacalai tesque) was dissolved in DMSO at 100 μM and stored at −20°C. U-73122 and U-73343 (Cayman Chemical, Ann Arbor, MI, USA) were dissolved in DMSO at 2 mM and stored at −20°C. Carbenoxolone (CBX; C4790, Sigma-Aldrich) was dissolved in DMSO at 100 mM and stored at −20°C.

Cell culture

Primary hippocampal neuron-astrocyte co-culture

Dissected hippocampi from E17 ICR mice were digested with 0.25% papain (Worthington Biochemical Corp., Lakewood, NJ, USA) containing 1% DNase (Roche, Basel, Switzerland) in Glucose mix [0.4% BSA (Sigma-Aldrich) and 0.04% L-cysteine (Nacalai tesque) in phosphate-buffered saline (PBS)] at 37°C for 5 min. Dissociated cells were seeded on poly-ethyleneimine (PEI, Sigma-Aldrich)-coated round glass coverslips (12 mm in diameter, 1×10^5 cells/cover slip, Matsunami Glass, Tokyo, Japan) in 24 well-plate in Neurobasal-A medium (GIBCO, Tokyo, Japan) containing 2% NeuroBrew-21 (Miltenyi Biotec, Tokyo, Japan), 1% L-glutamine (GIBCO), 5 U/mL penicillin and 5 μg/mL streptomycin (Nacalai tesque). Day *in vitro* (DIV) 10–15 cultures were used for experiments.

Primary hippocampal glial culture

Four hippocampi taken from two E17 ICR mice were digested with 0.25% papain containing 1% DNase in Glucose mix at 37°C for 5 min. Dissociated cells were seeded on PEI-coated 10-cm culture dishes in Dulbecco's Modified Eagle Medium (DMEM)/Ham's F12 medium (Sigma-Aldrich) containing 5% horse serum (GIBCO) and 5% fetal bovine serum (JRH Biosciences, Lenexa, KS, USA), 1% L-glutamine, 5 U/mL penicillin and 5 μg/mL streptomycin. Medium was changed every three days. After confluency, which took 7–10 days, cells were suspended with 0.05% trypsin in Ca and Mg free Hank's balanced salt solution (Nacalai tesque) and plated on poly-L-Lysine (PLL, Sigma-Aldrich) coated round glass coverslips (5×10^4 cells/cover slip) or PLL coated 6-well plate (3×10^5 cells/well) with the same culture medium. Within 2–5 days after the replating when cultures reached 70–90% confluency, cells were used for experiments.

Primary cortical glial culture

A cortical hemisphere taken from E17 ICR mouse was digested with 0.25% papain containing 1% DNase in Glucose mix at 37°C for 30 min. Dissociated cells were processed and used for experiments as is described for hippocampal glial culture.

Primary spinal cord glial culture

A spinal cord was isolated from an E17 ICR mouse by hydraulic extrusion (Richner et al., 2017) and digested with 0.25% papain containing 1% DNase in Glucose mix at 37°C for 20 min. Dissociated cells were processed and used for experiments as is described for hippocampal glial culture.

Cell lines

C6 (JCRB Cat#IFO50110, RRID:CVCL_0194), COS-7, HEK293T, HeLa and NIH/3T3 cell lines were seeded on 10-cm dishes in DMEM containing 10% fetal bovine serum, 5 U/mL penicillin and 5 μg/mL streptomycin. After confluency, cells were collected using 0.05% trypsin in Ca and Mg free HBSS and plated on Matrigel (BD Biosciences, NJ, USA)-coated round glass coverslips with the same culture medium at 5×10^4 cells/cover slip. Cultures at 70–90% confluency were used for Ca imaging.

Immunohistochemistry

Cells were fixed in 4% paraformaldehyde/PBS (Nacalai tesque) for 15 min, permeabilized with 0.25% Triton X-100 (FUJIFILM Wako Pure Chemical Corp., Osaka, Japan) in PBS for 10 min and blocked with 1% bovine

serum albumin (BSA, A9647, Sigma-Aldrich) in PBS for 1hr at room temperature (RT). Cells were incubated with primary antibodies (1:500 dilution in 1% BSA) overnight at 4°C and with secondary antibodies (1:1000 dilution in 1% BSA) for 1 h at RT. Primary antibodies used were: anti-NeuN (Cat# MAB377, Millipore, Tokyo, Japan, RRID:AB_2298772), anti-GFAP (Cat# ab53554, Abcam, Tokyo, Japan, RRID:AB_880202), and anti-Iba1 (Cat# 019-19741, FUJIFILM Wako Shibayagi Corp, Shibukawa, Japan; RRID:AB_839504). Secondary antibodies used were: Alexa Fluor 594 donkey anti-mouse IgG H&L (Cat# ab150108, Abcam, RRID:AB_2732073), Alexa Fluor 488 chicken anti-goat IgG H&L (Cat# A-21467, Molecular Probes, RRID:AB_141893), and Alexa Fluor 594 donkey anti-rabbit IgG (H+L) (Cat# A-21207, Thermo Fisher Scientific, RRID:AB_141637). Nuclei were stained with DAPI (sc-3598, Santa Cruz Biotechnology, Dallas, TX, USA). Images were obtained with an inverted microscope (IX71, Olympus, Tokyo, Japan) with a 20× objective (UApo/340, N.A. 0.75, Olympus) and a cooled-CCD camera (ORCA-ER, Hamamatsu Photonics, Hamamatsu, Japan).

Filipin staining

Cells were fixed with 4% paraformaldehyde/PBS for 15 min and stained with 50 mg/mL filipin (F9765, Sigma-Ardrich) in PBS for 30 min. The cells were then washed with PBS and observed with the same fluorescence microscope system as above with 330–385 nm band-pass excitation and 420–460 nm band-pass emission filters. Images were taken from 20 locations per sample, and signal intensity was obtained from 5 cells per field of view by placing a 33.3 × 33.3 μm-sized square region of interest (ROI) inside each cell.

Cell culture imaging

Coverslips holding cultured cells were mounted in a stainless-steel chamber (SCC12-D35-SET, Tokai Hit, Fujinomiya, Japan) containing HEPES-buffered saline (HBS; in mM, 20 HEPES, 115 NaCl, 5.4 KCl, 1 $MgCl_2$, 2 $CaCl_2$, 10 glucose, pH 7.4). A Ca indicator, Fura-2, was loaded to cells by incubation with 2.5 μM Fura-2-AM (Dojindo, Kumamoto, Japan) in HBS at 37°C for 10 min followed by three washes with HBS. Time-lapse imaging was performed with the fluorescence microscope described above. Fura-2 imaging was performed as described (Adachi et al., 2019) with a modification in the baseline correction method: asymmetrically reduced penalized least squares smoothing method (Baek et al., 2015) built in the TI Workbench software (Inoue, 2018) was used for baseline correction. Threshold for Ca transient detection was set as 6× standard deviation of the baseline. Oval ROIs were set on all cells identified by the Fura-2 staining in each field of view.

Gene transfection and YC3.60 imaging

Plasmid DNA encoding YC3.60 (Nagai et al., 2004) was introduced into hippocampal glial culture by electroporation using the Amaxa Basic Nucleofector kit for Primary Mammalian Glial Cells (Lonza Japan, Tokyo, Japan) according to the manufacturer's protocol with modifications. In brief, cultured astrocytes were stripped from dishes with 0.025% trypsin for 10 min at 37°C. 1.0×10^6 cells were centrifuged at 80 g for 10 min at RT. Collected cells were diluted in the nucleofection solution with 3 μg plasmid DNA and electroporated with the T-020 setting of the electroporator (Nucleofector 2b, Lonza Japan), followed by a recovery step with 500 μL equilibrated culture medium. Transfected astrocytes were divided into 12 equal portions and placed on PLL-coated round coverslips (12 mm in diameter). Equilibrated culture medium was added gently just after. Two–five days after transfection, cells at 60–80% confluency were used for Ca imaging. During this set of imaging experiments culture medium containing 25 mM HEPES (pH 7.40) was used as an extracellular medium rather than HBS because of the long recording periods (6 h). YC3.60 imaging was performed with the fluorescence microscope system described above with a 10× objective (UPlanApo, NA, 0.40, Olympus). YC3.60 was excited with light passed through a 426–496 nm band-pass filter, and image pairs of alternating emission wavelength (467–496 nm and 515–560 nm for CFP and YFP, respectively) were taken every 5 s. The fluorescence intensity ratio (F_{YFP}/F_{CFP}) was calculated at each time point in each ROI by dividing fluorescence intensity of YFP by that of CFP after background subtraction. Baseline determination was done as described for Fura-2 imaging, and threshold for event detection was set to 2× standard deviation of the baseline.

Cholesterol quantification

Cholesterol was quantified with Amplex™ Red Cholesterol Assay Kit (Invitrogen, Waltham, MA, USA) according to the manufacture's protocol. Cells were washed twice with ice cold PBS and then lysed in 200 μL reaction buffer. 50 μL of each sample was added to 50 μL assay solution containing 300 μM Amplex Red

reagent, 2 U/mL HRP and 2 U/mL cholesterol oxidase. After preincubation at 37°C for 30 min, fluorescence was measured using excitation at 560 nm and emission at 590 nm with a microplate reader (Synergy H1, Wakenyaku Co., Ltd., Kyoto, Japan). Relative amount of cholesterol was calculated using a standard curve obtained with the cholesterol standard solution.

Real-time PCR

Total RNA was isolated from hippocampal glial culture plated in a 6-well plate using ISOGEN II RNA extraction kit (NIPPON GENE, Tokyo, Japan) according to the manufacture's protocol. cDNA was constructed by reverse transcription using 200–300 ng isolated RNA, and real-time PCR was conducted using THUNDERBIRD SYBR qPCR kit (Toyobo, Osaka, Japan) according to the manufacture's protocol with StepOnePlus Real-Time PCR System (Applied Biosystems, Bedford, MA, USA). Primers used were: mouse *gfap* forward, 5′-TTGCTGGAGGGCGAAGAAAA-3′; reverse, 5′-TGCTTTTGCCCCCTCGGAT-3′; mouse *β-actin* forward, 5′-GCTCCTAGCACCATGAAGA-3′; reverse, 5′-ACTCCTGCTTGCTGATCCAC-3′.

Cell viability assay

Cell viability assay was performed using Apoptotic/Necrotic/Healthy Cells Detection Kit (PromoCell, Heidelberg, Germany) according to the manufacture's protocol. Cells were washed twice with binding buffer, and stained with FITC-Annexin V, ethidium homodimer III and Hoechst 33,342 for 30 min at RT. Images were taken as described in the "Immunohistochemistry" section. Twenty images were taken per sample and positive cell number in each image was averaged.

Ca imaging in brain slice

Hippocampal slices, 400 μm thickness, were prepared from 4- to 8-week-old Mlc1-tTA:tetO-YC-Nano50 female mice (Kanemaru et al., 2014) using a standard method (Samios and Inoue, 2014) and used within 12 h after preparation. Continuous superfusion of extracellular solution (artificial cerebrospinal fluid; ACSF; in mM, NaCl 124; KCl 2.5; NaH_2PO_4 1.25; $NaHCO_3$ 26; $MgCl_2$ 2; $CaCl_2$ 2; glucose 20; bubbled with 95% O_2 and 5% CO_2 gas mixture) at 3–5 mL/min in imaging chamber on the microscope stage is necessary for acute brain slice imaging. Because continuous superfusion of slices with cholesterol-containing ACSF was technically difficult, hippocampal slices were incubated in still ACSF containing 250 μM cholesterol or vehicle (water, 1:10 vol:vol) in ACSF, for 1–2 h in slice incubation chambers (Dorris et al., 2014), then transferred to imaging chamber on the microscope stage. Time-lapse imaging was performed with an in-house two-photon microscope (Inoue, 2018) mounted on an upright microscope (BX51, Olympus) with a 20× water immersion objective (XLUMPlanFI, N.A., 0.95, Olympus). Brain slices were continuously superfused with ACSF. An excitation laser of wavelength 860 nm (titanium-sapphire pulse laser, Mai Tai DeepSee, Spectra-Physics, Santa Clara, CA, USA) was used. The emission was divided with a 505-nm beam splitter and passed through a 440–480 nm or 500–550 nm band-pass filter for the CYP and YFP signals, respectively. Data were obtained every 5 s and converted to the relative change in fluorescence, F_{YFP}/F_{CFP}, with TI Workbench, then analyzed with the AQuA software (Wang et al., 2019) using the built-in cytosolic GCaMP6f *ex vivo* preset parameter with modifications: minimal pixel size, 25; seed growing threshold, 2; correct baseline trend, 2. Ca events of which duration (period above 10% of peak amplitude) was shorter than 20 s were discarded.

Lipid droplet staining

Cells were fixed with 4% paraformaldehyde/PBS for 15 min and stained with 1 mg/mL Nile red (N-1142, Thermo Fisher Scientific, Tokyo, Japan) in PBS for 30 min. After staining, cells were washed with PBS for 3 times and observed using a confocal microscope (FV-300, Olympus) equipped on an inverted microscope (IX-70, Olympus) with a 60× water immersion objective (UPlanSApo, N.A. 1.2, Olympus). Nile red was excited using a 561 nm diode-pumped solid-state laser (85-YCA-010-040, Melles Griot, Rochester, NY, USA), and the fluorescence was detected through a 565 nm long-pass filter. To quantify dot like structures, Nile red images were processed with a watershed segmentation algorithm (Vincent and Soille, 1991) equipped in TI Workbench, and particles consisting of more than 4 pixels of intensity larger than 300 (a.u.) were took into account.

QUANTIFICATION AND STATISTICAL ANALYSIS

For comparison between two groups, Mann-Whitney U test included in the ALGLIB library (www.alglib.net) implemented in TI Workbench was used unless otherwise indicated. For multiple groups,

Kruskal-Wallis test and post hoc Bonferroni corrected Mann-Whitney U test was performed with R (version 4.0.3; Ihaka and Gentleman, 1996) unless otherwise mentioned. Sample numbers were described in figure legends. p values less than 0.001, 0.01, 0.05 were indicated by ***, ** and *, respectively. Box and whisker plots indicate median as the horizontal line, interquartile range as the box and 10 and 90% ranges as the whiskers.